Published in final edited form as:
J Neurophysiol. 2008 May ; 99(5): 2390–2407. doi:10.1152/jn.00751.2007.

Sensitivity of Inferior Colliculus Neurons to Interaural Time Differences in the Envelope Versus the Fine Structure With Bilateral Cochlear Implants

Zachary M. Smith[1,2,4] and **Bertrand Delgutte**[1,2,3]

1*Eaton-Peabody Laboratory, Massachusetts Eye and Ear Infirmary, Boston, Massachusetts*

2*Speech and Hearing Bioscience and Technology Program, Harvard-MIT Division of Health Sciences and Technology, Cambridge, Massachusetts*

3*Research Laboratory of Electronics, Massachusetts Institute of Technology, Cambridge, Massachusetts*

4*Research and Applications, Cochlear Americas, Englewood, Colorado*

Abstract

Bilateral cochlear implantation seeks to improve hearing by taking advantage of the binaural processing of the central auditory system. Cochlear implants typically encode sound in each spectral channel by amplitude modulating (AM) a fixed-rate pulse train, thus interaural time differences (ITD) are only delivered in the envelope. We investigated the ITD sensitivity of inferior colliculus (IC) neurons with sinusoidally AM pulse trains. ITD was introduced independently to the AM and/or carrier pulses to measure the relative efficacy of envelope and fine structure for delivering ITD information. We found that many IC cells are sensitive to ITD in both the envelope (ITD_{env}) and fine structure (ITD_{fs}) for appropriate modulation frequencies and carrier rates. ITD_{env} sensitivity was generally similar to that seen in normal-hearing animals with AM tones. ITD_{env} tuning generally improved with increasing modulation frequency up to the maximum modulation frequency that elicited a sustained response in a neuron (tested ≤Hz). ITD_{fs} sensitivity was present in about half the neurons for 1,000 pulse/s (pps) carriers and was nonexistent at 5,000 pps. The neurons that were sensitive to ITD_{fs} at 1,000 pps were those that showed the best ITD sensitivity to low-rate pulse trains. Overall, the best ITD sensitivity was found for ITD contained in the fine structure of a moderate rate AM pulse train (1,000 pps). These results suggest that the interaural timing of current pulses should be accurately controlled in a bilateral cochlear implant processing strategy that provides salient ITD cues.

INTRODUCTION

Cochlear implantation is a widely used treatment for sensorineural deafness with > 100,000 adults and children implanted worldwide. While most cochlear implant users have only been implanted in one ear, bilateral implantation is rapidly becoming routine to restore the advantages of binaural hearing. However, commercially available cochlear implant sound processors have not been designed with binaural hearing in mind.

Binaural advantages for normal listeners include accurate localization of sound sources in the horizontal plane and improved speech reception in background noise (Blauert 1997; Durlach

Address for reprint requests and other correspondence: Z. M. Smith, Cochlear Americas, 400 Inverness Parkway, Suite 400, Englewood, CO 80112 (E-mail: zsmith@alum.mit.edu).

and Colburn 1978; Zurek 1993). The acoustic cues that lead to these advantages result from the physical separation of the two ears about the head and include interaural time and level differences (ITD and ILD). This study addresses issues of ITD coding with bilateral cochlear implants by studying the sensitivity of neurons to ITD using electric stimulation in an animal model. We focus on ITD because although bilaterally implanted subjects have good ILD discrimination (Grantham et al. 2008; Laback et al. 2004; van Hoesel and Tyler 2003), their ability to discriminate ITD is highly variable across subjects and comparable to normal performance only over a narrow range of stimulus parameters even in the best subjects, leaving much room for improvement in how this important binaural cue is encoded (Laback et al. 2007; Long et al. 2003; van Hoesel 2007; van Hoesel and Tyler 2003).

In a companion study (Smith and Delgutte 2007), we found that the ITD tuning of single units in the cat inferior colliculus (IC) for bilateral electric stimulation with low-rate, constant-amplitude pulse trains is as sharp at near-threshold intensities as for acoustic stimulation with broadband noise in normal-hearing animals. Such low-rate pulse trains have temporally punctate waveforms that make them ideal for revealing the intrinsic ITD sensitivity of binaural neurons, but they clearly differ from the more complex stimulation produced by cochlear implant sound processors. The present study focuses on ITD sensitivity for amplitude-modulated (AM) pulse trains that better mimic the types of stimulation used in clinical devices.

Cochlear implant sound processors typically split sound into multiple frequency bands and then use the filtered signals in each band to modulate the amplitude of current pulses delivered to tonotopically arranged intracochlear electrodes. For example, the popular continuous interleaved sampling (CIS) strategy (Wilson et al. 1991) uses the amplitude envelope of the filtered sound signal in each frequency channel to modulate the amplitude of a fixed-rate pulse train, which is temporally interleaved with the pulse trains in other channels to mitigate electrode interactions. In this scheme, as well as the majority of clinical processing strategies, the temporal fine structure of the original sound signal is discarded and only the amplitude envelope is delivered to the auditory nerve via the implanted electrodes. Thus the only ITD cues available to users of bilateral cochlear implants are contained in the amplitude envelope. While envelope cues in a limited number of frequency bands (e.g., 6–12) suffice for speech understanding in favorable acoustic environments (Shannon et al. 1995), they do not provide good speech reception in noise, fine pitch discrimination, and accurate localization of low-frequency sounds (Henning 1974; Henning and Ashton 1981; Qin and Oxenham 2003; Smith et al. 2002).

Neural sensitivity to ITD originates in the auditory brain stem. Neurons in the medial and lateral superior olive (MSO and LSO) create ITD tuning from convergent inputs from the contra- and ipsilateral ears. While MSO neurons are typically sensitive to ITD in the fine time structure of low-frequency sounds (Goldberg and Brown 1969; Yin and Chan 1990), a majority of LSO neurons are sensitive to ITD in the amplitude envelope of AM tones with high-frequency carriers (Joris and Yin 1995). LSO neurons are also highly sensitive to ILD (Boudreau and Tsuchitani 1968; Tollin and Yin 2005). Both MSO and LSO neurons have direct and indirect projections to the IC where neurons have ITD tuning that can resemble that in the MSO and LSO and can also be more complex (Batra et al. 1993; McAlpine et al. 1998; Yin and Kuwada 1983). Stimulation with broadband noise shows that ITD-sensitive IC neurons with low characteristic frequencies (CFs; <1 kHz) are primarily sensitive to ITD in the fine time structure, while neurons with high CFs (>3 kHz) are primarily sensitive to ITD in the envelope (Joris 2003).

The primary purpose of this paper is to determine the relative neural sensitivity to ITD in the amplitude envelope (ITD_{env}) versus the temporal fine structure (ITD_{fs}) with bilateral electric stimulation. Because ITD_{fs} is perceptually more salient than ITD_{env} in normal hearing

(Macpherson and Middlebrooks 2002; Wightman and Kistler 1992), neuronal sensitivity in the IC of normal hearing animals is generally greater for ITD_{fs} than for ITD_{env} (Batra et al. 1993; Griffin et al. 2005; Yin et al. 1984), and electric stimulation of the cochlea elicits precise temporal responses to electric pulses in the auditory nerve (Javel and Shepherd 2000; Moxon 1967; van den Honert and Stypulkowski 1987), we hypothesize that ITD-sensitive neurons will be more sharply tuned to ITD_{fs} than to ITD_{env} with electric stimulation. To test this hypothesis, we investigated the ITD sensitivity of IC neurons to AM pulse trains delivered via bilaterally implanted intracochlear electrodes. We found that the majority of neurons in the central nucleus of IC are sensitive to ITD_{env} with tuning similar to that seen for acoustic stimulation with AM tones in normal-hearing animals. We also found that many neurons are sensitive to ITD_{fs} at a moderate pulse rate (1,000 pps) and that this tuning is sharper than that for ITD_{env}. Preliminary reports have been presented (Smith and Delgutte 2003a,b, 2005a,b).

METHODS

Experimental procedures

Methods for animal preparation, electric stimulation, and single-unit recordings were as described in detail by Smith and Delgutte (2007). All surgical and experimental procedures were approved by the internal animal care and use committees of both the Massachusetts Eye and Ear Infirmary and the Massachusetts Institute of Technology. Briefly, cats were deafened by coadministration of kanamycin (300 mg/kg sc) and ethacrynic acid (25 mg/kg iv) 7–14 days prior to the experiment (Xu et al. 1993). For all animals, no auditory brain stem response was seen on the day of the experiment when stimulated with acoustic clicks (110 dB SPL). On the day of the experiment, after induction of anesthesia by Dial in urethane (75 mg/kg), stimulating electrodes were surgically implanted into each cochlea through the round window. The electrodes were either custom-made Pt/Ir ball electrodes (0.45 mm diam), or eight-contact electrode arrays with 0.75 mm spacing (Cochlear, Englewood, CO; ring-type contacts with 0.45 mm diam). In all experiments, we used a wide bipolar configuration (~5 mm between electrodes) with the active electrode inserted ~5 mm into the scala tympani and the return electrode (either another Pt/Ir ball or the most basal contact of the array) just inside the round window.

Part of the skull overlying the occipital cortex was removed to allow for partial aspiration of cortical tissue and access to the IC. Single-unit activity in the IC was recorded using either parylene-insulated tungsten stereotrodes (Microprobe, Potomac, MD; ~2 MΩ impedance), or 16-channel silicon probes (NeuroNexus Technologies, 100 or 150 μm spacing between contacts, 177 μm^2 site area). Recording electrodes were advanced through the IC either from dorsolateral to ventromedial in the coronal plane tilted 45° off the sagittal plane or vertically from dorsal to ventral (Smith and Delgutte 2007). Stimulus artifact was reduced in real time by means of an adaptive digital filter (Smith and Delgutte 2007).

Once a single unit was isolated, its threshold was measured with monaural and diotic pulses. The basic ITD sensitivity was then assessed with constant-amplitude pulse trains at 40 pps (Smith and Delgutte 2007). Following this preliminary characterization, binaural responses to AM pulse trains were studied. AM stimuli were made up of electric pulse trains at a rate of either 1,000 or 5,000 pps. Individual current pulses were biphasic (cathodic-anodic, 50 μs/phase). Pulse trains were sinusoidally amplitude modulated using modulation frequencies (f_{mod}) of 10–200 Hz and a 100% modulation depth. The “standard” stimulus was a 40-Hz/1,000-pps AM pulse train. Stimuli with dynamic ITDs have been used to efficiently study envelope ITD tuning of single units in normal-hearing animals (Yin et al. 1984). Here a dynamic ITD was imposed in the envelope of AM stimuli by making f_{mod} in the contralateral ear 1 Hz higher than in the ipsilateral ear (Fig. 1*A*). The interaural phase difference in the amplitude envelope (IPD_{env}) of this “binaural modulation beat” (BMB) stimulus takes all

possible values from −0.5 to +0.5 cycles over the 1-s beat period (Fig. 1*C*). The BMB stimulus was presented continuously for 30 s (30 beat cycles). The interaural timing of the carrier pulses was controlled independently and is shown for ITD_{fs} = 0 (synchronized carrier) in Fig. 1*B*. In some cases, ITD_{fs} tuning was measured simultaneously with ITD_{env} by systematically varying the static ITD_{fs} of the BMB stimulus (usually over 1 cycle of the 1,000-pps carrier in 100- or 200-μs steps). Unless otherwise stated, the stimulation current was 2 dB above the threshold current level required to elicit sustained responses with the standard AM stimulus in each neuron. All other dB current values are referenced to this threshold. In some units, the dependence of ITD_{env} tuning on stimulus level was also studied.

Data analysis

Spike times were processed to determine the discharge rate as a function of IPD_{env}. First, a period histogram was computed for 30 presentations of the 1-s modulation beat cycle using a 25-ms bin width. An example is shown in Fig. 1*D* for f_{mod} at 10 Hz. IPD_{env} functions were then computed from the period histograms by converting time to IPD_{env} cycles and then circularly convolving with a three-point smoothing kernel with values [0.25 0.5 0.25]. The IPD_{env} function derived from the PST histogram of Fig. 1*D* is shown in *E*. This function can also be expressed in terms of ITD_{env} by multiplying the IPD_{env} values by the period of f_{mod}. Positive values of IPD and/or ITD indicate contralateral-leading stimulation, whereas negative values indicate ipsilateral-leading stimulation. Note that because the 1-s beat cycle was analyzed with a 25-ms bin width, the resolution of our IPD_{env} curves is 1/40 cycle; at low modulation frequencies, this translates to a rather coarse resolution in ITD_{env} (e.g., 625 μs for 40-Hz modulation). We address this point in the DISCUSSION.

ITD_{fs} functions were obtained by presenting the BMB stimulus at several ITD_{fs} steps and plotting the average spike rate over the 30-s stimulus duration as a function of ITD_{fs} for a specific IPD_{env} (typically 0) chosen to get near-maximal firing rates.

Sensitivity to ITD was quantified by computing the mean interaural phase and the vector strength (Goldberg and Brown 1969) of the IPD_{env} and ITD_{fs} functions. The vector strength takes on a value between 0 and 1 and indicates how much the spike distribution over one cycle of IPD differs from uniform. Neurons are considered to be ITD sensitive if the vector strength of their IPD function is statistically significant ($P < 0.001$) as determined by the Rayleigh test of uniformity (Mardia and Jupp 2000).

Characteristic delay (CD) and characteristic phase (CP) were estimated in neurons that were tested at several values of f_{mod}. Mean interaural phase as a function of f_{mod} was fit with a regression line using a weighted least-squares procedure (Kuwada et al. 1987). Each phase point was weighted by the product of the vector strength and mean firing rate. Only data that passed the linearity test described by Yin and Kuwada (1983), with a criterion of $P < 0.005$, were analyzed for CD and CP. For these neurons, the slope of the regression line gives the CD and the intercept gives the CP.

We used a metric from signal detection theory to quantify ITD discrimination thresholds based on spike counts from single neurons in a way that can be compared with psychophysical thresholds (Jiang et al. 1997; Shackleton et al. 2003). Our metric D was a slight modification of standard separation (Sakitt 1973; Simpson and Fitter 1973)

$$D_{\mathrm{ITD},\mathrm{ITD}+\Delta\mathrm{ITD}} = \frac{|\mu_{\mathrm{ITD}} - \mu_{\mathrm{ITD},\Delta\mathrm{ITD}}|}{\sqrt{(\sigma^2_{\mathrm{ITD}} + \sigma^2_{\mathrm{ITD}+\Delta\mathrm{ITD}})/2}}$$

where μ_{ITD} and μITD + ΔITD are the means of the spike counts and σITD and σITD + ΔITD their respective SDs. This metric expresses the difference in spike counts elicited by stimuli

with two different ITDs in units of their combined SD. We use the arithmetic mean of variances rather than the geometric mean used in the original definition of *D* to avoid problems when the spike-count variance is 0 for one of the two ITDs. Standard separation is analogous to *d′* which is often used to quantify discrimination in psychophysical studies (Green and Swets 1966). The just-noticeable difference (JND) in ITD was defined as the ΔITD, from a reference ITD of 0, needed for the standard separation to reach a value of 1. This criterion corresponds to ~76% correct in a two-interval, two-alternative forced choice discrimination task.

RESULTS

Results are based on responses of 47 IC neurons to bilateral electric stimulation of the cochlea with AM pulse trains in 17 deafened cats. While most neurons only exhibited onset discharges to constant-amplitude pulse trains at rates >300 pps (Smith and Delgutte 2007), applying low-frequency AM (<200 Hz) reintroduced ongoing firing at moderate and high pulse rates (1,000 and 5,000 pps). ITDs were applied to the modulation waveform and carrier pulses independently to test the hypothesis that neuronal selectivity would be greater for ITD in the temporal fine structure (ITD_{fs}) than for ITD_{env}. Neural sensitivities to ITD_{env} and ITD_{fs} were characterized at several intensities, modulation frequencies, and pulse rates.

The breakdown of the number of neurons sensitive to each type of ITD is given in Table 1. Of the 47 neurons studied, 46 responded throughout the duration of AM stimuli when probed with a 1,000-pps carrier at 10 or 40 Hz AM. Of these 46 neurons, 35 (76%) were sensitive to ITD in the amplitude envelope. This is slightly lower than the 86% of neurons that were previously found to be sensitive to ITD for low-rate (40 pps), unmodulated pulse trains (Smith and Delgutte 2007). Thirty one of these ITD_{env}-sensitive neurons were tested for additional ITD sensitivity in the fine structure with a carrier rate of 1,000 pps. 17/31 neurons were sensitive to both ITD_{env} and ITD_{fs}, while the remaining 14/31 neurons were only sensitive to ITD_{env}. Finally, seven neurons that showed good ITD_{fs} tuning at 1,000 pps were also tested at 5,000 pps. Only one neuron exhibited any significant ITD_{fs} sensitivity at this higher rate.

Envelope ITD sensitivity at 40 Hz

Neurons with sustained responses to AM stimuli were tested for sensitivity to ITD_{env} using a dynamic ITD_{env} stimulus (BMB). Because ITD_{fs} was usually fixed at 0 μs, this stimulus has mismatched envelope and carrier ITDs except for the brief moments when ITD_{env} passes through 0 μs. If a neuron showed no ITD_{env} sensitivity with zero ITD_{fs}, it was tested with other ITD_{fs} to make sure the lack of ITD_{env} sensitivity did not result from a choice of unfavorable ITD_{fs}. A total of 44 neurons were tested with AM pulse trains using a 1,000-pps carrier and f_{mod} = 40 Hz at 2 dB above threshold. These stimulus parameters were chosen because most neurons in the IC respond well to 40 Hz AM, and 1,000 pps lies within the range of pulse rates used in today's cochlear-implant processors.[1] Thirty three of these neurons were found to be ITD_{env} sensitive by the Rayleigh test, and the majority of these (27/33) had peaked-shaped ITD_{env} tuning (Fig. 2*A*), whereas the remaining 6 neurons had trough-shaped tuning (Fig. 2*B*). Gaussian functions with either positive or negative amplitude were fit to peak- and trough-shaped ITD_{env} curves, respectively, and quantitative measures of ITD tuning (best IPD_{env}, half-width, ITD of maximum slope, etc.) were obtained from the fitted Gaussians. The Gaussian fits were also used to scale and shift the ITD_{env} curves in Fig. 2, *A* and *B*, so that they are all centered at 0 with a half-width and a height of 1. The peak-shaped curves are largely symmetric around the best ITD, whereas many of the trough-shaped curves show a sharper edge on the side contralateral to the worst ITD (toward positive ITDs from trough) than on the ipsilateral side.

[1]Two additional neurons tested with 10 Hz modulation are not shown in Fig. 2

The distributions of ITD_{env} tuning metrics are shown in Fig. 2, *C–G*, separately for peak-shaped (gray bars) and trough-shaped (black lines) curves. However, summary statistics reported below group both types of IPD_{env} tuning because there are not enough trough units to make strong statistical comparisons between the two. The distribution of vector strengths, which is a measure of the strength of IPD_{env} tuning (Fig. 2*C*), is very broad, with a mean of 0.51 and SD of 0.28 for ITD_{env}-sensitive neurons. The distribution of "best" IPD_{env} (Fig. 2*D*), which is defined as the location of the peak or trough of the Gaussian fit, is tightly clustered near 0 cycle with a mean of −0.02 cycles (corresponding to −0.5 ms for 40-Hz AM) and a SD of 0.09 cycles (2.3 ms). All six trough-type neurons had negative worst IPD_{env}. To characterize the precision of ITD_{env} tuning, we used the *half-width*, the width of the tuning curve at half the range of firing rates (sometimes called "full-width at half-max"). The half-width of each ITD_{env} tuning curve (Fig. 2*E*) was calculated from the Gaussian fits $(\text{half}-\text{width}=2\sigma\sqrt{2\ln 2})$. Trough-type responses tended to have larger half-widths than peak-type responses. The geometric mean half-width (3.3 ms, or 0.13 cycles of the 40-Hz modulator) is much larger than the ±350 μs range of ITDs naturally encountered by a cat, suggesting poor ITD_{env} discrimination for the average IC neuron at this low AM frequency. However, wide ITD_{env} tuning may not preclude good discrimination as long as there is a large change in discharge rate within the range of naturally occurring ITDs. Using the fitted Gaussians, we determined the place of maximum slope of ITD_{env} tuning curves, where the sensitivity is high.[2] Because there are two ITD_{env} where the slope approaches maximum (1 on each side of the best/worst ITD), we only characterized the maximum closest to $ITD_{env} = 0$. Figure 2*F* shows that, for the majority of neurons (27/33), maximum slopes occur outside of the ±350 μs range of naturally occurring ITDs for cat, further suggesting poor discrimination of ITD_{env} by IC neurons.

To test this idea more directly, neural ITD_{env} discrimination thresholds, a.k.a. just noticeable differences (JNDs) in ITD_{env}, were estimated from rate responses of single-units using the procedures described in METHODS. Briefly, spike count statistics at each ITD_{env} step were used to determine the smallest ITD_{env} step from 0 that could be reliably detected by an ideal observer. ITD_{env} JNDs were obtained for 31/33 neurons; the other two had unmeasurable ITD_{env} JNDs because the standard separation *D* never reached criterion. The distribution of ITD_{env} JNDs is shown in Fig. 2*G* on a logarithmic scale. The geometric mean of the distribution (excluding the 2 neurons with unmeasurable JNDs) is 1.0 ms, and the best ITD_{env} thresholds are near 400 μs. This result confirms that ITD_{env} discrimination thresholds of IC neurons for 40-Hz modulation are poor compared with the natural range of ITDs encountered by the cat.

Effect of stimulus intensity on envelope ITD tuning

In 12 neurons with peak-shaped ITD_{env} tuning, ITD_{env} sensitivity was studied for several stimulus intensities with the standard AM stimulus parameters (carrier rate = 1,000 pps, f_{mod} = 40 Hz). Current level (in dB) was varied equally in both ears, typically in 1 dB steps, starting from threshold to 3–6 dB above threshold. Figure 3*A* shows ITD_{env} tuning curves for an example neuron at five intensities. With increasing intensity, the peak firing rate increases and ITD_{env} tuning broadens. Also the peak of the ITD_{env} function shifts toward more ipsilateral leading (negative) ITD_{env}. This shift results in a relatively stable location of the steep downwards slope of the function near 0 μs despite widening with increasing intensity. These trends are better appreciated by looking at changes with stimulus intensity over the entire sample of neurons. Figure 3*B* shows the best IPD_{env} for each neuron as a function of intensity. As for the example neuron in Fig. 3*A*, best IPD_{env} shifts toward more negative values (ipsilateral leading) for the majority of neurons. A linear regression (thick dashed line) reveals a significant negative correlation ($r = -0.32$, $P = 0.037$) between intensity and best IPD_{env}

[2]Sensitivity is best where *D*, not necessarily slope, is maximal. Because variance grows with spike count, maximum sensitivity usually occurs at lower spike counts than those at the steepest slope (Tollin 2007).

across the population, despite considerable scatter. Also as in Fig. 3*A*, ITD_{env} half-width increases with intensity for most neurons (Fig. 3*C*), and the correlation is significant ($r = 0.36$, $P = 0.017$). Figure 3*D* shows that there is also a significant shift toward move negative values in the location of the maximum slope of ITD_{env} curves with intensity ($r = -0.33$, P = 0.030). However, the slope of the regression line is shallower for the location of maximum slope than for the best ITD, indicating that the point of maximum sensitivity is more stable to changes in intensity than the best ITD.

Neural ITD_{env} JNDs are shown as a function of intensity in Fig. 3*E*. Although there is no significant trend for the population data ($r = -0.002$, P = 0.99) due to the wide variation in JNDs across neurons, ITD_{env} JNDs seem to improve (decrease) with increasing intensity for most neurons. To quantify this observation, a straight line was fit to the data for each neuron with measurable JNDs. Across the population, the slopes were significantly <0 (*t*-test, $P = 0.010$) with a mean slope of −0.15 ms/dB ($\sigma = 0.15$) indicating that, on average, ITD_{env} JNDs decrease with increasing intensity (this was the case for all 10 neurons that had measurable JNDs at multiple intensities). Thus neural discrimination thresholds generally improved (smaller JNDs) with increasing stimulus intensity despite the broadening of the ITD_{env} functions. Because the neural thresholds depend on a significant change in firing rate between the reference ITD_{env} and a neighboring ITD_{env}, the reduction in JNDs at higher intensities could be caused by increases in slope and/or shifts in the location of the steep slope toward the 0 reference ITD. For the neuron in Fig. 3*A* (dashed lines in Fig. 3, *B*–*E*), the location of the steep slope shifted further away from 0 rather than toward 0, so the improvement in JND must be due to increases in slope relative to the variability of firing rates.

Effect of modulation frequency and carrier rate on ITD_{env} sensitivity

Because the modulation frequencies at the output of a cochlear-implant sound processor will vary over a wide range for stimulation by natural sounds, ITD_{env} tuning was tested as a function of modulation frequency (f_{mod}) between 20 and 160 Hz in several neurons with peak-shaped ITD_{env} tuning. Figure 4*A* shows IPD_{env} tuning curves for an example neuron stimulated at eight modulation frequencies with the same 1,000-pps carrier rate. The neuron responds poorly at the lowest f_{mod} tested (20 Hz); at higher f_{mod}, both the best IPD_{env} and the shapes of the tuning curves are fairly stable, although the peak firing rates vary substantially. Figure 4*B* shows the peak firing rate of each IPD_{env} curve as a function of modulation frequency, a measurement we call “peak rate modulation transfer function” (prMTF). This neuron responds best to BMB stimuli at $f_{mod} = 60$ Hz. The vector strength (Fig. 4*C*) is statistically significant ($P < 0.001$) for all f_{mod} and increases from a low value at 20 Hz to reach a plateau at ≥60 Hz. The half-width of the IPD_{env} curve (Fig. 4*D*) is relatively stable for all f_{mod} except 20 Hz when expressed in units of modulation cycles. Therefore the half-width decreases with increasing f_{mod} when expressed in ms (Fig. 4*E*). Mean interaural phase (Fig. 4*F*) decreases slowly with increasing f_{mod}. The dependence of mean phase on f_{mod} is fairly well characterized by a straight line (fit with the weighted least-squares procedure described in METHODS), indicating that the neuron has a CD (−1.08 ms). Finally, the neural ITD_{env} JND of this neuron (Fig. 4*G*) generally decreases with increasing f_{mod}, consistent with parallel drops in ITD_{env} half-width, and is always substantially below one half modulation cycle (- - -), which represents the maximum possible JND.

We studied the effect of f_{mod} on ITD_{env} tuning in 15 neurons using a pulse rate of 1,000 pps and in 11 neurons using a pulse rate of 5,000 pps. Stimuli were presented at the same current level for both pulse rates. Stimulation at rates above the upper frequency limit of phase locking to pure tones in the auditory nerve (4,000–5,000 kHz) has been proposed as a means of improving speech reception with cochlear implants (Rubinstein et al. 1999). Such high-rate

stimulation might also be beneficial for binaural hearing by mitigating the possible confounding effects of conflicting ITD_{env} and ITD_{fs} cues delivered by today's processors.

Figure 5 *A–C*, shows ITD_{env} half-widths, ITD_{env} JNDs, and prMTF as a function of f_{mod} for our entire sample of neurons. The *top* and *middle rows* show data from individual neurons for stimuli with pulse rates of 1,000 and 5,000 pps, respectively. The *bottom row* shows the population mean data for the two pulse rates. ITD_{env} half-width (Fig. 5*A*) tends to decrease monotonically with increasing f_{mod} between 20 and 80 Hz for both pulse rates. This trend continues to hold for a majority of the neurons >80 Hz, but some neurons deviate from monotonicity. The population mean ITD_{env} half-widths (Fig. 5*A*, *bottom*) are very similar for the 1,000- and 5,000-pps carrier rates. The thin dotted line in Fig. 5*A*, *bottom*, shows the equation κ/f_{mod} (where $\kappa = 0.11$ is a proportionality constant). This line is very close to the mean data for both pulse rates, meaning the mean half-widths are roughly a constant fraction of the modulation period, although the 5,000-pps curve falls slightly faster for low f_{mod}. A two-way ANOVA on the logarithms of the half-widths showed a main effect of f_{mod} (continuous predictor) as expected [$F(1,198) = 223$, $P < 0.001$] but no significant effect of carrier rate [$F(1,198) = 1.6$, $P = 0.21$] and no interaction.

Neural ITD_{env} JNDs were computed from each neuron's ITD_{env} tuning curves as a function of f_{mod} (Fig. 5*B*). The dotted line in each panel of Fig. 5*B* shows $1/(2f_{mod})$, which is the maximum measurable JND. Unmeasurable JNDs are not plotted. In general, the neural JNDs decrease with increasing f_{mod}, consistent with the decrease in half-width in Fig. 5*A*. For the 1,000-pps carrier, the geometric mean ITD_{env} JND across the population drops steadily with increasing f_{mod} over the entire range (Fig. 5*B*, *bottom*). Mean ITD_{env} JNDs for the 5,000-pps carrier closely parallel the JNDs for the 1,000-pps carrier ≤80 Hz but become nearly flat >80 Hz unlike the decreasing trend seen for the 1,000-pps carrier. A two-way ANOVA on the logarithms of the JNDs showed a main effect of f_{mod} [$F(1,143) = 61.5$, $P < 0.001$] and a significant interaction between f_{mod} (continuous predictor) and carrier rate [$F(1,143) = 4.64$, $P = 0.033$], reflecting the different dependence of JNDs on f_{mod} for the two rates.

The difference in mean ITD JNDs between the two carrier rates at higher f_{mod} is unexpected because the mean ITD_{env} half-widths are very similar (Fig. 5*A*, *bottom*). However, these differences may be explained by taking into account the prMTFs shown in Fig. 5*C*. For both carrier rates, most prMTFs for individual neurons are band-pass, although the best f_{mod} varies considerably among neurons. The mean prMTFs across the population (Fig. 5*C*, *bottom*) are also band-pass for both carrier rates with best modulation frequencies near 40–60 Hz. However, the magnitude of the mean prMTF is greater for the 1,000-pps carrier than for the 5,000-pps carrier, and this difference is most prominent at higher f_{mod} where the mean prMTF for 5,000 pps shows a sharp drop-off. These differences in mean prMTFs reflect in part wider bandwidths of individual prRMTFs at 1,000 pps compared with 5,000 pps and in part a greater proportion of higher best f_{mod} at 1,000 pps. In any case, the lower firing rates in response to higher f_{mod} for the 5,000- pps carrier rate may largely account for the plateau in mean ITD JNDs seen in Fig. 5*B*.

A further difference between the two carrier rates emerges when the proportion of measurable ITD_{env} JNDs is analyzed (Fig. 6*A*). For the 1,000-pps carrier, the proportion of neurons with measurable ITD_{env} JNDs is ~70% across the entire range of f_{mod} tested. For the 5,000-pps carrier, the proportion is similar to that for 1,000 pps for f_{mod} between 20 and 60 Hz but tends to fall at higher f_{mod} to reach ~40% at 160 Hz. This is also probably a result of the lower peak firing rates at higher f_{mod} for the 5,000-pps carrier compared with the 1,000-pps carrier (Fig. 5*C*). A similar tendency for neural MTFs to drop more rapidly at higher pulse rates has been reported in the auditory cortex for monaural electric stimulation of the cochlea (Middlebrooks and Lee 2004).

The mean interaural phase of neurons that were tested over a range of modulation frequencies was analyzed. Only data for the 1,000-pps carrier was examined here because more neurons were tested at 1,000 pps than at 5,000 pps. Fourteen of 15 neurons had a linear phase-f_{mod} relationship ($P < 0.005$) and were used to calculate distributions of CP and CD. The distribution of CP (Fig. 6*B*) is centered near 0, with a mean of 0.03 ± 0.13 (SD) cycles, consistent with the observation that these neurons had peak-shaped IPD_{env} functions. The distribution of CD is broad, with a mean of −0.03 ± 0.91 (SD) ms.

ITD sensitivity to the temporal fine structure

Sensitivity to ITDs in the temporal fine structure (ITD_{fs}) was measured simultaneously with ITD_{env} sensitivity by introducing static ITDs in the carrier of the dynamic ITD_{env} stimulus. Tests of ITD_{fs} sensitivity were always made at f_{mod} = 40 Hz, most frequently with a carrier rate of 1,000 pps. Figure 7*A* shows IPD_{env} curves for an example neuron at 10 different IPD_{fs} steps covering the 1,000-μs period of the 1,000-pps carrier. This neuron is sensitive to ITDs introduced to both the amplitude envelope and the temporal fine structure of the stimulus. It responds well to ITD_{fs} between −100 and +200 μs and IPD_{env} near 0 cycles. These curves can be combined into a two-dimensional pseudocolor display of discharge rate against both IPD_{env} and IPD_{fs} (Fig. 7*B*). ITD_{fs} tuning curves were derived from this display by taking one column and converting IPD_{fs} into ITD_{fs} by scaling by the 1,000-μs carrier period. The ITD_{fs} tuning curve for IPD_{env} = 0 cycles (Fig. 7*C*) shows sharp tuning centered at +100 μs. The half-width of ITD_{fs} tuning is 284 μs (from fitted Gaussian), compared with 2.57 ms for the half-width of ITD_{env} tuning. Note that, although IPD tuning is narrower in the modulation dimension, ITD tuning is narrower in the carrier dimension due to the large disparity in period between the AM and the carrier (25 vs. 1 ms, respectively).

A total of 31 ITD_{env}-sensitive IC neurons were tested for sensitivity to ITD_{fs} at a carrier rate of 1,000 pps. Roughly half of these neurons (17/31) showed significant ITD_{fs} tuning ($P < 0.001$, as assessed with the Rayleigh coefficient of the IPD_{fs} vector strength). A histogram of ITD_{fs} half-widths for the 31 neurons is shown in Fig. 8*A*. ITD_{fs} sensitive neurons are shown by ■, and □ to the right indicates the neurons that were not sensitive to ITD_{fs} at 1,000 pps. The mean ITD_{fs} half-width for the 17 ITD_{fs}-sensitive neurons was 287 μs, which is narrower than the 691 μs mean half-width observed for 40-pps constant-amplitude pulse trains in a larger sample of IC neurons (Smith and Delgutte 2007). A histogram of ITD_{fs} JNDs (from a reference ITD_{fs} of 0 μs) for the population is shown in Fig. 8*B*. The mean ITD_{fs} JND for ITD_{fs}-sensitive neurons is ~100 μs, which is comparable to the 118 μs mean ITD JND for low-rate constant-amplitude pulse trains (Smith and Delgutte 2007).

ITD_{fs} tuning for the standard stimulus (1,000 pps, 40 Hz) is much sharper, when present, than ITD_{env} tuning over the range of f_{mod} tested (20–160 Hz; Fig, 5A). The mean ITD_{fs} JND is also significantly lower than the mean ITD_{env} JND (Fig. 5*B*) over the range of f_{mod} tested. While ITD_{env} tuning would presumably continue to sharpen at higher f_{mod}, the peak firing rate of most neurons would be expected to drop off sharply for f_{mod} >300 Hz based on IC data for monaural electric stimulation of the cochlea (Snyder et al. 2000). Thus ITD_{env} tuning may never “catch up” with ITD_{fs} even by using higher modulation frequencies.

Relating ITD_{fs} tuning to ITD tuning with low-rate, constant-amplitude pulse trains

Why is only a subset of neurons sensitive to ITD_{fs} at 1,000 pps, while most binaural neurons are sensitive to ITD_{env} and nearly 90% of neurons in a larger sample were sensitive to ITD for constant-amplitude, 40-pps pulse trains (Smith and Delgutte 2007)? About half of the neurons in the Smith and Delgutte (2007) study had ITD half-widths >500 μs, which is half the period of our standard 1,000-pps carrier, and thus would be unlikely to show ITD_{fs} sensitivity at this carrier rate. This corresponds roughly to the proportion of ITD_{fs} -insensitive neurons we

observed, suggesting the hypothesis that ITD_{fs} sensitive neurons may just be those that have the sharpest ITD tuning. To test this hypothesis, we investigated possible differences in basic ITD tuning between the ITD_{fs}-sensitive and -insensitive neurons.

Basic ITD tuning characteristics measured with 40-pps constant- amplitude pulse trains include the ITD of maximum slope (ITD_{MS}), the half-rise (width of the rate-ITD function about ITD_{MS} between 25 and 75% normalized spike rate), and the physiological modulation depth (PMD; normalized change in spike rate within the natural range of ITD for the cat). ITD_{MS} and half-rise are used for comparison in lieu of best ITD and half-width because the latter are only defined for peak- and trough-shaped ITD curves, whereas the former are also defined for monotonic and biphasic ITD curves. These basic ITD tuning characteristics, as well as ITD_{env} half-width and electrode depth, were compared between ITD_{fs}-sensitive (n = 16) and ITD_{fs}-insensitive neurons (n = 15) using two-sample *t*-tests. Table 2 shows the means and SDs, and the result of the *t*-test, for each metric. ITD_{fs}-sensitive neurons have significantly narrower half-rises, ITD_{MS} closer to 0 (and within the natural range of ITD), and higher PMDs than ITD_{fs}-insensitive neurons, consistent with the hypothesis that this subset of neurons is more sharply tuned. ITD_{fs}-sensitive neurons also have significantly narrower ITD_{env} half-widths and were recorded at shallower electrode depths than ITD_{fs}-insensitive neurons, suggesting that these neurons would have lower CFs in normal-hearing animals.

Figure 8*C* shows basic ITD half-rise (measured with 40-pps pulse trains) plotted against ITD_{env} half-width for 40-Hz modulation for the population of neurons. Although there is no significant correlation between these two metrics ($r = 0.14$, $P = 0.50$), their combination provides a fairly clear segregation of ITD_{fs}-sensitive from ITD_{fs}-insensitive neurons: ITD_{fs}-sensitive neurons (*) cluster in the *lower left corner* of the plot. ITD_{fs}-sensitive neurons with larger basic ITD half-rise tend to have smaller ITD_{env} half-width, whereas those with larger ITD_{env} half-width tend to have smaller basic ITD half-rise. Overall, these analyses support the hypothesis that ITD_{fs}-sensitive neurons are fundamentally more sharply tuned to ITD than ITD_{fs}-insensitive neurons.

ITD_{fs} tuning at high carrier rates

In a small number of ITD_{fs}-sensitive neurons, the effect of using a higher pulse rate on ITD_{fs} tuning was tested. The standard stimulus had a carrier rate of 1,000 pps and therefore a period of 1,000 μs. The higher pulse rate was 5,000 pps with a period of 200 μs. ITD tuning would have to be very sharp to see a modulation of the response within the ±100 μs possible range of ITD_{fs} with a 5,000-pps carrier. Very few (3/92) neurons in our sample studied with 40-pps constant-amplitude pulse trains had ITD half-widths <200 μs (Smith and Delgutte 2007).

Figure 9, *A* and *B*, shows the IPD_{env}-IPD_{fs} tuning display for an example neuron with f_{mod} = 40 Hz for pulse rates of 1,000 and 5,000 pps, respectively. ITD_{fs} tuning at 1,000 pps is relatively sharp for this neuron (half-width = 108 μs, vector strength = 0.85) and the best ITD_{fs} is near 0 μs (Fig. 9*C*). When the carrier rate is increased to 5,000 pps (Fig. 9*B*), IPD_{env} tuning curves become very similar for all IPD_{fs} tested, indicating that ITD_{fs} tuning is essentially eliminated (Fig. 9*D*, vector strength = 0.02 and not statistically significant). The effect of carrier rate on ITD_{fs} tuning was tested in seven neurons with good ITD_{fs} tuning at 1,000 pps; in each case, ITD_{fs} tuning was eliminated or severely reduced with the 5,000-pps carrier. The mean vector strength was 0.68 for the 1,000-pps carrier and only 0.13 for 5,000 pps. Six of the seven vector strength measures for the 5,000-pps carrier were not significant at the 0.1% level.

Whole waveform ITD sensitivity for AM stimuli

All measures of ITD sensitivity reported so far involved independent manipulations of envelope and fine structure ITD. We also tested sensitivity to ITD imposed on the whole

waveform of AM pulse trains in which envelope and carrier ITDs are matched. For acoustic stimulation, this would be a more natural stimulus because ITDs are normally contained in both the envelope and the fine structure in free field. While current processors for cochlear implants only deliver ITD in the envelope, whole-waveform ITDs might be implemented in future processing strategies to better mimic normal acoustic stimulation.

Figure 10*A* shows the dynamically derived ITD_{env} tuning curve (ITD_{fs} = 0 μs) for the same neuron as in Fig. 9*A* using 40-Hz AM and 1,000-pps carrier rate. The colored *inset* of Fig. 10*A* shows the joint ITD_{env}-ITD_{fs} tuning for this neuron; the main plot of Fig. 10*A* is a horizontal section (ITD_{fs} = 0 μs) through the colored *inset*. Because the 1,000-pps carrier rate has a period of 1 ms, the ITD_{fs} curve for this neuron over the range from −5 to +5 ms (Fig. 10*C*) is the same as the ITD_{fs} curve from Fig. 9*C* repeated every 1 ms. Comparison of Fig. 10*C* with Fig. 10*A* illustrates how much sharper the ITD_{fs} tuning is than ITD_{env} tuning. Whole waveform ITD (ITD_{wav}) tuning was also measured with static ITD stimuli for this neuron (Fig. 10*E*, blue). The shape of the ITD_{wav} curve is very close to the product of the ITD_{env} and ITD_{fs} curves (Fig. 10*E*, green line): the response peaks every 1,000 μs as does the ITD_{fs} curve but only over a range of ITDs of about the same width and shape as the ITD_{env} curve. However, the envelope of the ITD_{wav} curve is more symmetric ~0 ITD than the ITD_{env} curve, which is slightly offset toward negative ITDs. This may be because the ITD_{env} curve was measured dynamically, whereas the ITD_{wav} curve was measured with static stimuli. In any case, within the range of relevant ITDs for a cat or a human, the ITD_{wav} sensitivity of this neuron is clearly dominated by its sensitivity to ITD_{fs}.

That the whole-waveform ITD curve can be approximated by the product of the ITD_{env} and ITD_{fs} curves as in Fig. 10*E* would be predicted mathematically if the effects of ITD_{env} and ITD_{fs} on neural responses were *separable*, i.e., if the response as a function of both ITD_{env} and ITD_{fs} could be expressed as the product of a function of ITD_{env} alone and a function of ITD_{fs} alone. The joint responses as a function of ITD_{env} and ITD_{fs} (as in Fig. 7*B* and Fig. 10*A*) were analyzed with singular value decomposition (SVD) to assess their separability (Pena and Konishi 2001). The SVD of a completely separable response has only one nonzero singular value, and the original response can be perfectly reconstructed from the external product of two vectors (in this context representing the independent sensitivities to ITD_{env} and ITD_{fs}). We assessed the degree to which each distribution is separable by determining the fraction of the energy of the joint distribution contained in the first singular value for each ITD_{fs}-sensitive neuron. For example, the fractional energy in the first singular value for the distribution of Fig. 10*A* is 97.3%, indicating a high degree of separability and explaining the observed resemblance between the whole-waveform ITD curve and the product of the ITD_{env} and ITD_{fs} curves for this neuron. Across our sample of 16 ITD_{fs}-sensitive neurons, the mean fractional energy in the first singular value was 87.9 ± 5.7%, indicating that a multiplicative model, with separable ITD_{env} and ITD_{fs} tunings, accounts for ~88% of the variance in the joint ITD_{env}-ITD_{fs} tuning space.

Figure 10, *right*, show results for another ITD_{fs}-sensitive neuron. The joint ITD_{env} and ITD_{fs} tuning function for this neuron (Fig. 10*B*, *inset*) is less separable than that for the neuron of Fig. 10*A* as shown by the marked tilt in the high-amplitude region. SVD analysis confirms the lesser separability of tuning for this neuron, with a fractional energy of 84.6% in the first singular value. As expected, multiplying the ITD_{env} and ITD_{fs} curves (green line in Fig. 10*F*) gives a relatively poor prediction of the measured ITD_{wav} curve (blue line in Fig. 10*F*) with the best ITD occurring near −1 ms in the prediction versus 0 ms in the data. Responses to the ITD_{wav} stimulus can also be predicted by resampling the joint ITD_{env}-ITD_{fs} distribution along the diagonal line representing equal ITD_{env} and ITD_{fs}. The prediction based on resampling the joint ITD_{env}-ITD_{fs} tuning function (red line in Fig. 10*F*) better matches the

measured ITD_{wav} curve than the multiplicative prediction based on the separability assumption (green line).

In summary, sensitivity to ITD in the whole waveform can be predicted from joint measurements of ITD_{env} and ITD_{fs} sensitivities. For a majority of neurons that have nearly independent sensitivities to ITD_{env} and ITD_{fs}, the prediction of ITD_{wav} sensitivity can be obtained more easily from separate measurements of these two sensitivities.

Phenomenological model of electric ITD tuning

To gain some insight into the mechanisms that underlie the ITD sensitivity of IC neurons for bilateral electric stimulation, we developed a phenomenological model that captures key trends in the data. The model consists of a cascade of stages that convert the electric current waveforms delivered to each ear into the firing probability of a single IC neuron. By varying ITD as in our experiments, rate-ITD functions are derived by integrating the spike probability over time to get the predicted firing rate at each ITD.

Figure 11 shows a block diagram of our model; the parameter values used are given in Table 3. The model includes a highly simplified peripheral stage describing auditory-nerve responses to electric stimulation, an interaural coincidence detector giving rise to ITD sensitivity, and an envelope processing model similar to that developed by Nelson and Carney (2004) for IC neurons. Peripheral processing (*stage 1*) is modeled by subtracting a constant threshold from the input waveform and then half-wave rectifying. The resulting waveform is then convolved with an excitatory postsynaptic potential (EPSP) of the form: $\alpha_e t e^{-t/\tau e}$, where α_e is a scale factor, τ_e is the time constant. This convolution implements a low-pass filter and serves to add temporal jitter and limit phase locking to the carrier at high pulse rates. The binaural processor (*stage 2*) consists of an internal delay imposed on the output of the contralateral ear to model to neuron's best ITD followed by a multiplication of the signals from the two ears to approximate interaural coincidence detection as in the Jeffress (1948) model. In *stage 3*, the output of the coincidence detector splits into two parallel branches. The first branch is excitatory and goes directly into a summation stage representing synaptic integration in the IC. The signal in the second branch is delayed (*synaptic*, 1 ms) and convolved with an inhibitory postsynaptic potential (IPSP) of the form: $-\alpha_i t e^{-t/\tau i}$, where α_i is a scale factor, and τi is the time constant. The negative sign makes the second branch inhibitory. The two branches are finally summed and half-wave rectified to obtain the probability of spiking in the IC neuron. The inhibitory branch in *stage 3* serves to block sustained firing at high pulse rates and high modulation frequencies.

The model captures key aspects of the data for both constant-amplitude and AM pulse trains, including: the reduction in sustained responses to constant-amplitude pulses with increasing pulse rate (Smith and Delgutte 2007; Snyder et al. 1995), the restoration of sustained responses to high-rate pulse trains by low-frequency AM, the decrease in ITD_{env} half-width with increasing modulation frequency, the increase in ITD_{env} half-width with increasing stimulus intensity, sharper tuning to ITD_{fs} than ITD_{env}, and the loss of ITD_{fs} sensitivity at very high pulse rates.

In the following examples of model responses to various electric stimuli, the peak stimulus intensity is expressed in decibels relative to the model threshold. So if an AM pulse train stimulus is 1 dB re threshold, then only pulses occurring during the peaks of the amplitude envelope exceed threshold.

Figure 12*A* shows the model responses to pulse trains of different carrier rates with an ITD equal to the *internal delay* of the model neuron at 1 dB re threshold. These responses represent the spike probabilities as a function of time and can be compared with PST histograms of

measured IC responses. The first five panels show the output of the model for constant-amplitude pulse trains with rates ranging from 40 to 1,000 pps. For 40 and 160 pps, the responses are sustained and locked to the individual stimulus pulses. For 320 pps, the response remains locked to the individual stimulus pulses, but firing probability is high at the onset and then is low throughout the remainder of the stimulus. For 500 and 1,000 pps, the spike probability is only greater than zero during a brief onset transient. The *bottom panel* shows the model output for a 1,000-pps pulse train with 40-Hz sinusoidal AM. Low-frequency AM restores a sustained response that is now phase-locked to the 40-Hz amplitude peaks of the stimulus. The key element of the model that creates a transition between sustained and onset-only responses is the delayed inhibition in *stage 3*. Because the time constant of the inhibition (τ_i = 2 ms) is an order of magnitude longer than that for the excitation (τ_e = 0.1 ms), the inhibition produced by one pulse builds up gradually and overlaps with the excitation produced by the next pulse for pulse rates >200 pps. At lower pulse rates, inhibition and excitation do not interact because they are interleaved in time. The temporal interaction between excitation and inhibition also imposes an upper limit on modulation frequencies that can elicit sustained responses to AM stimuli. A similar interplay between excitation and inhibition was proposed to account for neural responses to SAM tones in the MSO of the mustache bat (Grothe 1994).

Envelope ITD functions for the model were calculated as a function of modulation frequency (Fig. 12*B*) and overall intensity (Fig. 12*D*) for AM pulse trains with 1,000-pps carriers. Consistent with the neural results, ITD_{env} half-width decreases with increasing f_{mod} (Fig. 12*C*) and increases with increasing intensity (Fig. 12*E*). In the model, the width and shape of ITD_{env} tuning are primarily dependent on the width and shape of the suprathreshold peaks in each AM cycle. By increasing f_{mod}, the width of the suprathreshold portion of the modulation envelope narrows and thus ITD_{env} half-width narrows. Similarly by increasing the stimulus intensity, more pulses within each AM cycle lie above threshold and thus the ITD_{env} half-width increases. Finally, whole waveform ITD curves from the model are shown in Fig. 12*F* for 40-Hz AM pulse trains at 1 dB re threshold with carrier rates of 1,000 and 5,000 pps. For the 1,000-pps carrier (*top*), ITD tuning to the fine structure creates a 1,000-μs periodicity in the ITD function that is much narrower than the wide ITD_{env} tuning that gives the function is overall shape. For the 5,000-pps carrier (*bottom*), ITD_{fs} is essentially lost, and only ITD tuning to the envelope remains. These results are consistent with the neural data (Fig. 9 and Fig. 10). In the model, ITD_{fs} tuning is lost at 5,000 pps because of low-pass filtering by the EPSP (τ_e = 0.1 ms) before coincidence detection.

DISCUSSION

We studied single-neuron responses to amplitude-modulated trains of electric current pulses in the IC of anesthetized cats with bilateral cochlear implants. Sensitivity to envelope ITD was found to be similar in many respects to that seen with acoustic stimulation. In agreement with results using acoustic stimulation (Batra et al. 1993), the half-width of ITD_{env} curves decreased with increasing modulation frequency such that half-width was nearly constant when expressed in units of modulation phase. Neurons that had the best sensitivity to ITDs in low-rate constant-amplitude pulse trains were also the most likely to be sensitive to ITD_{fs} with a 1,000-pps carrier. Neural ITD_{fs} selectivity was relatively sharp when compared with ITD_{env} tuning for 1,000-pps carriers but was eliminated at the high carrier rate of 5,000 pps. This is similar to acoustic stimulation where neural sensitivity to ITD_{fs} in the IC drops rapidly >1,500 Hz (Joris 2003; Yin et al. 1984) and ITD_{env} JNDs to sinusoidal AM tones are poorer than JNDs for pure tones at the AM envelope frequency (Griffin et al. 2005).

Sensitivity to envelope ITD

The vast majority of neurons in the IC were sensitive to ITD_{env} at modulation frequencies that elicited a sustained response. The decrease in ITD_{env} half-width with increasing f_{mod} was consistent with constant IPD_{env} half-width over the range of f_{mod} tested (20–160 Hz). A similar result has been reported in high-CF neurons of the IC of the awake rabbit using acoustic stimulation with SAM tones over a higher range of f_{mod} (300–700 Hz) (Batra et al. 1993). As for acoustic stimulation (Batra et al. 1993; Yin et al. 1984), the dependence of best ITD_{env} on f_{mod} was fairly linear for the majority of our neurons, so that these neurons had a well-defined CD. The range of CDs was comparable to that seen acoustically for modulation frequencies <150 Hz (Batra et al. 1993), although the small size of our sample precludes a detailed comparison.

Our IPD_{env} curves were sampled at a resolution of 1/40 cycle, which translates to rather coarse sampling in ITD_{env} for low modulation frequencies (e.g., 625 μs for 40-Hz modulation). It is conceivable that this coarse ITD_{env} sampling at low f_{mod} might have obscured sharp features in the ITD_{env} curves, particularly near 0 ITD. We believe that this possibility is very unlikely for the following reasons. First, the ITD_{env} curves were all smooth and well-behaved (Fig. 1*E*, Fig. 3*A*, and Fig. 4*A*) and highly consistent across neurons (Fig. 2*A*). Because the points at which we sample the ITD_{env} curves differ in relation to each neuron's best ITD_{env}, the shapes of the ITD_{env} curves would not be expected to be so consistent if they contained micro features. Second, the ITD_{env} curves maintain their shape as the modulation frequency is increased (Fig. 5), and the ITD_{env} resolution improves in proportion to f_{mod} (e.g., 156-μs resolution for 160-Hz modulation). Finally, none of the whole-waveform ITD curves we measured using a resolution of 250 μs showed any unusual feature (Fig. 10). These curves always consisted of a rapid oscillation reflecting ITD_{fs} sensitivity modulated by a smooth envelope resembling our dynamic ITD_{env} curves. Despite these arguments, a definitive resolution of the question of whether ITD_{env} curves might contain microfeatures would require repeating our dynamic IPD_{env} measurements using lower beat frequencies.

We found that using a higher f_{mod} leads to sharper ITD_{env} tuning and smaller ITD_{env} JNDs. Although values of f_{mod} >160 Hz were not systematically tested, previous studies with monaural electric stimulation suggest that there is a limit near 200–300 Hz above which most IC neurons would have a diminished sustained response (Snyder et al. 1995, 2000), similar to the rate limit seen previously (Smith and Delgutte 2007) with bilateral constant-amplitude pulse trains. If this upper limit is not a result of sampling bias or an artifact of anesthesia, then employing values of f_{mod} much greater than those tested in this study may not lead to better ITD_{env} sensitivity. Such an upper limit is not seen with acoustic stimulation, where some IC neurons give sustained responses to AM tones for f_{mod} of 1,000 Hz and above (Batra et al. 1989; Krishna and Semple 2000; Schreiner and Langner 1988).

Because ITD_{env} tuning half-width seems to be directly related to the width of each cycle of the amplitude envelope, temporal sharpening of the envelope might improve ITD_{env} tuning, while avoiding high stimulus rates that result in mostly onset responses in the IC. Temporal sharpening of the amplitude envelope is also achieved in acoustic studies of binaural hearing by the stimulus transposition technique, in which a high-frequency sinusoidal carrier is modulated by a half-waverectified, low-frequency stimulus (van de Par and Kohlrausch 1997). Transposed stimuli provide better behavioral (Bernstein and Trahiotis 2002) and neural (Griffin et al. 2005) ITD_{env} discrimination thresholds than conventional AM stimuli.

Although we did not observe a significant difference in ITD_{env} half-widths between carrier rates of 1,000 and 5,000 pps, ITD_{env} JNDs were somewhat poorer >80 Hz, and the proportion of units with measurable ITD_{env} JNDs was lower for the 5,000-pps carrier. Thus the theoretical benefit of using higher carrier rates to increase the upper limit of envelope frequencies that can

be delivered with a cochlear implant may be partly offset by a moderate degradation of ITD_{env} sensitivity with higher carrier rates.

Sensitivity to fine structure ITD

While stimulation with a constant-amplitude 1,000-pps pulse train carrier elicited predominantly onset responses in IC neurons, low-frequency AM of the carrier restored sustained responses to bilateral stimulation, consistent with previous observations for monaural stimulation (Snyder et al. 2000). Despite a general lack of phase locking to the 1,000-pps carrier, over half of our IC neurons were sensitive to ITD_{fs} at this carrier rate when AM was imposed on the stimulus. One possible interpretation of this finding is that ITD_{fs} sensitivity arises at a level lower than the IC (such as the SOC) as suggested in previous studies of acoustic stimulation with AM tones in high-frequency neurons (Batra et al. 1993; Yin et al. 1984), while the mechanism responsible for the upper limit of phase locking occurs after ITD_{fs} processing. Our phenomenological model is consistent with this interpretation because the upper frequency limit to sustained responses is determined by the time constant τ_i of the inhibitory synapse occurring after the binaural coincidence detector, while the upper limit of ITD_{fs} sensitivity is determined by the time constant τ_e of the excitatory synapse preceding the coincidence detector. However, Colburn et al. (2007) developed an MSO neuron model without inhibition that can also simulate both the lack of sustained responses at higher pulse rates and the restoration of sustained responses and ITD sensitivity by introducing lowfrequency AM. In their model, the suppression of sustained responses is caused by the dynamics of ionic membrane channels, particularly low-threshold potassium channels. The two mechanisms (inhibition and hyperpolarizing membrane channels) are not mutually exclusive, and both may be necessary to account for all the data.

The ranges of ITD_{fs} half-widths and neural JNDs with the 1,000-pps carrier are consistent with the values previously obtained in the best neurons for low-rate (40 pps) constantamplitude pulse trains (Smith and Delgutte 2007). Neurons that are sensitive to ITD_{fs} tend to have sharp ITD tuning for low-rate constant amplitude pulse trains, while neurons that are insensitive to ITD_{fs} had broader ITD tuning. This is an intuitive result because the 1,000-pps carrier imposes a limited physical range (±500 μs) of ITD on the stimulus. It is also interesting to consider that ITD_{fs} -sensitive neurons tended to be located at shallower electrode depths in our dorsal-to-ventral penetrations and thus would lie in lower-CF regions of the IC in normalhearing animals (Table 2). Because MSO neurons mostly target low-CF regions of the IC (Adams 1979; Loftus et al. 2004), this might suggest that ITD_{fs} -sensitive IC neurons preferentially receive inputs from the MSO. However, in our previous study with bilateral electric stimulation (Smith and Delgutte 2007), there was no correlation between sharpness of ITD tuning and electrode depth in the IC, so this idea may be too simplistic. Mechanisms underlying the substantial variability in ITD tuning among IC neurons with electric stimulation are poorly understood.

Unlike acoustic stimulation, where phase locking in the auditory nerve begins to degrade above ~1,500 Hz (Johnson 1980; Joris et al. 1994), electric stimulation can produce significant phase locking well above 5,000 pps (Dynes and Delgutte 1992). The loss of ITD_{fs} sensitivity we observed at the higher carrier rate (5,000 pps) may result from the coincidence window of the ITD-processing neurons being relatively wide compared with the 200-μs period of the carrier, or alternatively may reflect a loss of phase locking beyond the auditory nerve in the binaural circuits that process ITD. The loss of ITD_{fs} sensitivity with high-frequency stimulation is also seen with acoustic hearing (Joris 2003; Yin et al. 1984). However, with electric stimulation, this effect can be observed within individual neurons since electric stimulation allows stimuli of any frequency to stimulate the same region of the cochlea, whereas in normal-hearing animals, the rapid increase in neural thresholds for frequencies above a neuron's CF imposes an upper limit on the frequencies that can be tested for ITD_{fs} sensitivity in any individual

neuron. Future studies will need to determine where between 1,000 and 5,000 pps the upper rate limit of ITD_{fs} sensitivity occurs in IC neurons with electric stimulation and whether this limit differs from that seen for acoustic stimulation.

Comparison of envelope and fine-structure ITD sensitivity

The result that IPD_{env} half-widths are nearly constant for a given neuron over a wide range of f_{mod} supports the notion that ITD_{env} sensitivity may have more to do with the instantaneous intensities of the stimulus at each ear rather than with the interaural timing of the amplitude envelopes. We showed previously that changing the rate of a constant-amplitude pulse train does not have a large effect on the half-width of ITD tuning (Smith and Delgutte 2007), but here with AM pulse trains, increasing f_{mod} proportionately decreased the half-width of ITD_{env} tuning. Varying f_{mod} changes both the rate and slope of each modulation cycle, so we cannot eliminate the possibility that the slope of the amplitude envelope is what determines the width of ITD_{env} tuning. Note also that the carrier pulses have infinite slope while the envelope has a slow rise-time. Future experiments using trapezoidal AM might help to separate the two factors.

Another line of evidence distinguishing ITD_{env} and ITD_{fs} sensitivities comes from measurements of neural sensitivity to ITD imposed on the whole waveform (Fig. 10, *E* and *F*). To a first-order approximation, these responses can be predicted from the product of separable sensitivities to ITD_{env} and ITD_{fs} , each of which can be measured by holding the other at a fixed value. There are, however, limits to the idea that ITD_{env} and ITD_{fs} sensitivities are independent. First, independence may no longer hold if the modulation and carrier frequencies were less disparate than in our measurements (40 Hz vs. 1,000 pps). Second, ITD_{fs} sensitivity for 1,000-pps carriers must vanish at very low f_{mod} as inferred from the lack of sustained responses to constant-amplitude pulse trains.

The phenomenological model presented in this paper may provide insight into the underlying factors that contribute to ITD_{env} and ITD_{fs} tuning. In the model, the width and shape of envelope ITD tuning with AM pulse trains are primarily controlled by the width and shape of each cycle of the stimulus AM that exceeds threshold. For fine structure ITD tuning with constant-amplitude or AM pulses, it is the width of the EPSP, or temporal jitter before binaural coincidence detection, that determines the width of ITD tuning.

Phenomenological model for ITD tuning

A relatively simple, phenomenological model of electric ITD tuning was created with the aim of better understanding the factors that influence electric ITD tuning at the level of the IC. The general structure of the model is broadly consistent with the organization of the auditory pathway and similar to that of existing models of IC responses to acoustic stimulation (Cai et al. 1998; Nelson and Carney 2004). Specifically, the model consists of three cascaded stages: a peripheral processor, a binaural coincidence detector, and an envelope processor. The peripheral processor roughly mimics the responses of auditory nerve fibers to electric stimulation. It is simpler than previous peripheral models of electric stimulation (Bruce et al. 1999, 2000) and only consists of a threshold followed by convolution with an EPSP. These effectively act to create a narrow dynamic range of stimulation and limit phase-locking at high pulse rates. The binaural processor is implemented as multiplication between a delayed input from the contralateral side and an undelayed input from the ispsilateral side. This architecture is comparable to Jeffress-type models of binaural coincidence detection (Jeffress 1948) and mimics the operation of the MSO when operating on spike probabilities (Batra and Yin 2004; Goldberg and Brown 1969; Yin and Chan 1990). The envelope processor implements the interaction between excitation from the output of the binaural coincidence detector with delayed inhibition from the same output. Possible anatomical substrates for an ITD-sensitive

inhibitory input to the IC, include projections from the dorsal nucleus of the lateral lemniscus (Adams and Mugnaini 1984; Brugge et al. 1970) and intrinsic inhibitory connections within the IC (Oliver et al. 1994). The envelope processor stage of the model, with the interaction of short excitation with delayed, long-lasting inhibition, is similar to existing models of IC responses to AM acoustic stimuli (Nelson and Carney 2004).

The model captures several aspects of the data in this and our previous report (Smith and Delgutte 2007), including: the reduction in sustained responses to constant-amplitude pulse trains with increasing pulse rate, the restoration of sustained responses to high-rate pulse trains by low-frequency AM, the decrease in ITD_{env} half-width with increasing modulation frequency, the increase in ITD_{env} half-width with increasing stimulus intensity, sharper tuning to ITD_{fs} than ITD_{env}, and loss of ITD_{fs} tuning at very high pulse rates. Aspects of the data that are not captured by the model include: the saturation of ITD functions for constant-amplitude pulse trains at high stimulus intensities (Fig. 5 in Smith and Delgutte 2007), shifts in best ITD_{env} with changes in overall intensity (Fig. 3*B*), shifts in best ITD (for constant-amplitude pulse trains) with changes in ILD (Fig. 6 in Smith and Delgutte 2007), and stochastic responses. Because the model is deterministic, it only predicts the mean discharge rate and not variability and thus cannot be used to predict ITD discrimination thresholds. Some of these limitations could be dealt with by more carefully modeling responses to electric stimulation observed in the auditory nerve. For example, the threshold stage of our peripheral model could be replaced by a more complex stage consisting of a dynamic threshold, intensity-dependent latency, and stochastic spiking (Bruce et al. 1999). Other model limitations, for example the dependence of best ITD_{env} on intensity, may require changes to the binaural processor itself. For our purposes, however, the simple model suffices to capture the major trends in the data, and our data with AM stimuli are too limited to allow meaningful testing of more elaborate model structures. Even in its simple form, the model is useful for understanding the basic mechanisms that possibly underlie neural ITD sensitivity with electric stimulation and can also be used to predict responses to stimuli not tested in vivo.

Comparison with behavioral data from bilaterally implanted human subjects

Agreement between our results and psychophysical reports of ITD sensitivity for AM stimuli in bilaterally implanted human subjects is mixed. van Hoesel and Tyler (2003) measured behavioral ITD JNDs for an 800-pps carrier both with and without sinusoidal AM in three subjects. While none of the subjects had measurable ITD JNDs for the unmodulated pulse train, 55-Hz modulation of the pulse carrier restored ITD_{wav} sensitivity in all three subjects tested. One of these subjects was tested with ITDs presented in the envelope only as well as ITDs in the whole waveform; this increased the JND from 120 to 290 μs, suggesting the subject must have benefited from fine-structure cues in the whole-waveform condition. In another study of lateralization of short trapezoidal AM stimuli (Majdak et al. 2006), stimuli with whole waveform ITD were generally more strongly lateralized than those restricted to envelope ITD for carrier rates below an upper limit. This upper rate limit for carrier contributions to lateralization varied substantially across subjects and could reach 800 pps in some subjects. Several other studies have reported across-subject differences in the ability to use ongoing ITD_{fs} cues at high pulse rates (van Hoesel 2007). Together these studies suggest that up to a certain carrier rate, ITD discrimination for AM stimuli benefits from the inclusion of ITD in the carrier, even at rates that, in some subjects, yield unmeasurable ITDs when not modulated. These psychophysical observations are qualitatively similar to our neural results in cat IC. We previously found that neural ITD sensitivity for constant-amplitude pulse trains degrades with increasing pulse rates due to the gradual loss of a sustained response (Smith and Delgutte 2007), and here we show that amplitude modulating a 1,000-pps pulse train restores ITD_{fs} sensitivity in a majority of neurons by eliciting sustained responses.

Behavioral data on ITD_{env} discrimination as a function of modulation frequency for AM pulse trains subjects are only available from one study that used three subjects (van Hoesel 2007). In contrast to our results that show decreasing neural ITD_{env} JNDs with increasing f_{mod} (20–160 Hz), their psychophysical results, using a 6,000-pps carrier, show increasing ITD_{env} JNDs with increasing f_{mod} from 100 to 400 Hz. However, it is hard to draw firm conclusions from this comparison because the behavioral thresholds were measured in 100-Hz steps, and there is only one overlapping f_{mod} (100 Hz) between the two datasets. A possible physiological explanation for the degradation in behavioral ITD_{env} sensitivity at ≥200 Hz is the reduced numbers of neurons giving sustained responses at these modulation frequencies (Snyder et al. 1995, 2000). Future studies need to investigate both behavioral ITD_{env} sensitivity at additional f_{mod} <200 Hz and neural ITD_{env} sensitivity at f_{mod} >160 Hz to test this interpretation. Some of the neural studies need to be done in awake animals to test whether the loss of sustained responses to electric stimulation at higher pulse rates and f_{mod} is dependent on anesthesia. Behavioral data from bilaterally implanted animals such as cats would also be valuable to address possible species differences.

Significance for bilateral cochlear implant processing strategies

The neural responses in this study show tuning to envelope ITD similar to that seen in normal-hearing animals using AM tones. Over the range of modulation frequencies tested (≤160 Hz), IC neurons are more sharply tuned to ITD in the fine time structure of 1,000-pps AM pulse trains than in the amplitude envelope, although ITD_{fs} sensitivity is essentially eliminated at a higher carrier rate of 5,000 pps. ITD_{env} sensitivity in our study is likely to have been overestimated because our stimuli all had 100% AM depth, which is considerably higher than the modulation depths at the output of cochlear implant speech processors. Processors typically modulate pulse amplitude in each channel between threshold and the maximum comfortable level. We expect the reduced modulation depths produced by clinical processors to broaden ITD_{env} tuning, thereby exacerbating the contrast between the good ITD_{fs} sensitivity and the poor ITD_{env} sensitivity we observed with 100% modulation of 1,000-pps carriers.

Based on our single neuron results, we suggest that a bilateral cochlear implant strategy that successfully conveys ITD cues should control the precise timing of current pulses based on the fine timing of the sound sources at each ear. van Hoesel and Tyler (2003) implemented such a strategy but found it yielded little or no benefit over the standard clinical strategy for sound localization and speech reception in noise when tested in five bilaterally implanted subjects. One possible explanation is that to be effective, a fine-structure-based strategy may require each electrode channel to stimulate a highly specific population of neurons, an ability that may be limited by the large channel interactions observed with contemporary scala tympani electrodes (Boex et al. 2003; Chatterjee and Shannon 1998; Shannon 1983). Because the stimulation in neighboring channels is temporally interleaved, channel interactions effectively increase the pulse rates seen by individual neurons and may therefore reduce the ability of the binaural processor to make use of ITD_{fs} cues. A further caveat with fine-structure-based strategies is that only about half of our neurons were sensitive to ITD_{fs} with 1,000-pps carriers, so the decoding stages beyond the IC would have to be able to selectively “attend” to the subpopulation of sensitive neurons to effectively process the available ITD information.

An alternative processing strategy would use carrier rates above the upper limit of sensitivity to ITD_{fs} (e.g., 5,000 pps) to avoid creating conflicting ITD_{fs} and ITD_{env} cues. However, any benefits arising from the ability to encode higher modulation frequencies with such a high-rate strategy would be at least partially mitigated both by the somewhat poorer neural ITD_{env} JNDs seen at higher f_{mod} for the 5,000-pps carrier compared with the 1,000-pps carrier and by the poor behavioral ITD_{env} JNDs at modulation frequencies >200 Hz (van Hoesel 2007). With either strategy, further benefit from improved sensitivity to envelope ITD may potentially be

achieved by temporally sharpening the amplitude envelope as in transposed stimuli (Bernstein and Trahiotis 2002; van de Par and Kohlrausch 1997), albeit with the possible side effect of distorting speech information. Clearly many interacting peripheral and central factors will influence the effectiveness of future processors designed to improve ITD sensitivity with bilateral cochlear implants.

ACKNOWLEDGMENTS

We thank C. Miller for surgical assistance, K. Hancock for computer support, and S. Colburn and D. Eddington for valuable comments on the manuscript.

GRANTS

This work was supported by National Institute of Deafness and Other Communications Diseases Grants R01 DC-005775 and P30 DC-005209 as well as T32 DC00038, which provided partial support for Z. M. Smith.

REFERENCES

Adams JC. Ascending projections to the inferior colliculus. J Comp Neurol 1979;183:519–538. [PubMed: 759446]

Adams JC, Mugnaini E. Dorsal nucleus of the lateral lemniscus: a nucleus of GABAergic projection neurons. Brain Res Bull 1984;13:585–590. [PubMed: 6098348]

Batra R, Kuwada S, Stanford TR. High-frequency neurons in the inferior colliculus that are sensitive to interaural delays of amplitude-modulated tones: evidence for dual binaural influences. J Neurophysiol 1993;70:64–80. [PubMed: 8395589]

Batra R, Kuwada S, Stanford TR. Temporal coding of envelopes and their interaural delays in the inferior colliculus of the unanesthetized rabbit. J Neurophysiol 1989;61:257–268. [PubMed: 2918354]

Batra R, Yin TC. Cross correlation by neurons of the medial superior olive: a reexamination. J Assoc Res Otolaryngol 2004;5:238–252. [PubMed: 15492883]

Bernstein LR, Trahiotis C. Enhancing sensitivity to interaural delays at high frequencies by using “transposed stimuli”. J Acoust Soc Am 2002;112:1026–1036. [PubMed: 12243151]

Blauert, J. Spatial Hearing: The Psychophysics of Human Sound Localization. Cambridge, MA: MIT Press; 1997.

Boex C, de Balthasar C, Kos MI, Pelizzone M. Electrical field interactions in different cochlear implant systems. J Acoust Soc Am 2003;114:2049–2057. [PubMed: 14587604]

Boudreau JC, Tsuchitani C. Binaural interaction in the cat superior olive S segment. J Neurophysiol 1968;31:442–454. [PubMed: 5687764]

Bruce IC, Irlicht LS, White MW, O’Leary SJ, Clark GM. Renewal-process approximation of a stochastic threshold model for electrical neural stimulation. J Computat Neurosci 2000;9:119–132.

Bruce IC, White MW, Irlicht LS, O’Leary SJ, Dynes S, Javel E, Clark GM. A stochastic model of the electrically stimulated auditory nerve: single-pulse response. IEEE Trans Biomed Eng 1999;46:617–629. [PubMed: 10356868]

Brugge JF, Anderson DJ, Aitkin LM. Responses of neurons in the dorsal nucleus of the lateral lemniscus of cat to binaural tonal stimulation. J Neurophysiol 1970;33:441–458. [PubMed: 4314734]

Cai H, Carney LH, Colburn HS. A model for binaural response properties of inferior colliculus neurons. I. A model with interaural time difference-sensitive excitatory and inhibitory inputs. J Acoust Soc Am 1998;103:475–493. [PubMed: 9440334]

Chatterjee M, Shannon RV. Forward masked excitation patterns in multielectrode electrical stimulation. J Acoust Soc Am 1998;103:2565–2572. [PubMed: 9604350]

Colburn, HS.; Chung, Y.; Zhou, Y.; Brughera, A. Models of neural responses to bilateral electrical stimulation. In: Kollmeier, B.; Klump, G.; Hohmann, V.; Langemann, U.; Mauermann, M.; Uppenkamp, S.; Verhey, J., editors. Hearing—From Sensory Processing to Perception. Berlin: Springer; 2007. p. 495-504.

Durlach, NI.; Colburn, HS. Binaural phenomena. In: Carterette, E.; Friedman, MP., editors. Handbook of Perception. New York: Academic; 1978. p. 365-466.

Dynes SB, Delgutte B. Phase-locking of auditory-nerve discharges to sinusoidal electric stimulation of the cochlea. Hear Res 1992;58:79–90. [PubMed: 1559909]

Goldberg JM, Brown PB. Response of binaural neurons of dog superior olivary complex to dichotic tonal stimuli: some physiological mechanisms of sound localization. J Neurophysiol 1969;32:613–636. [PubMed: 5810617]

Grantham DW, Ashmead DH, Ricketts TA, Haynes DS, Labadie RF. Interaural time and level difference thresholds for acoustically presented signals in post-lingually deafened adults fitted with bilateral cochlear implants using CIS+ processing. Ear Hear 2008;29:33–44. [PubMed: 18091105]

Green, DM.; Swets, JA. Signal Detection Theory and Psychophysics. New York: Krieger; 1966.

Griffin SJ, Bernstein LR, Ingham NJ, McAlpine D. Neural sensitivity to interaural envelope delays in the inferior colliculus of the guinea pig. J Neurophysiol 2005;93:3463–3478. [PubMed: 15703234]

Grothe B. Interaction of excitation and inhibition in processing of pure tone and amplitude-modulated stimuli in the medial superior olive of the mustached bat. J Neurophysiol 1994;71:706–721. [PubMed: 8176433]

Henning GB. Detectability of interaural delay in high-frequency complex waveforms. J Acoust Soc Am 1974;55:84–90. [PubMed: 4815755]

Henning GB, Ashton J. The effect of carrier and modulation frequency on lateralization based on interaural phase and interaural group delay. Hear Res 1981;4:185–194. [PubMed: 7240025]

Javel E, Shepherd RK. Electrical stimulation of the auditory nerve. III. Response initiation sites and temporal fine structure. Hear Res 2000;140:45–76. [PubMed: 10675635]

Jeffress LA. A place theory of sound localization. J Comp Physiol Psychol 1948;41:35–39. [PubMed: 18904764]

Jiang D, McAlpine D, Palmer AR. Detectability index measures of binaural masking level difference across populations of inferior colliculus neurons. J Neurosci 1997;17:9331–9339. [PubMed: 9364078]

Johnson DH. The relationship between spike rate and synchrony in responses of auditory-nerve fibers to single tones. J Acoust Soc Am 1980;68:1115–1122. [PubMed: 7419827]

Joris PX. Interaural time sensitivity dominated by cochlea-induced envelope patterns. J Neurosci 2003;23:6345–6350. [PubMed: 12867519]

Joris PX, Carney LH, Smith PH, Yin TC. Enhancement of neural synchronization in the anteroventral cochlear nucleus. I. Responses to tones at the characteristic frequency. J Neurophysiol 1994;71:1022–1036. [PubMed: 8201399]

Joris PX, Yin TC. Envelope coding in the lateral superior olive. I. Sensitivity to interaural time differences. J Neurophysiol 1995;73:1043–1062. [PubMed: 7608754]

Krishna BS, Semple MN. Auditory temporal processing: responses to sinusoidally amplitude-modulated tones in the inferior colliculus. J Neurophysiol 2000;84:255–273. [PubMed: 10899201]

Kuwada S, Stanford TR, Batra R. Interaural phase-sensitive units in the inferior colliculus of the unanesthetized rabbit: effects of changing frequency. J Neurophysiol 1987;57:1338–1360. [PubMed: 3585471]

Laback B, Majdak P, Baumgartner WD. Lateralization discrimination of interaural time delays in four-pulse sequences in electric and acoustic hearing. J Acoust Soc Am 2007;121:2182–2191. [PubMed: 17471732]

Laback B, Pok SM, Baumgartner WD, Deutsch WA, Schmid K. Sensitivity to interaural level and envelope time differences of two bilateral cochlear implant listeners using clinical sound processors. Ear Hear 2004;25:488–500. [PubMed: 15599195]

Loftus WC, Bishop DC, Saint Marie RL, Oliver DL. Organization of binaural excitatory and inhibitory inputs to the inferior colliculus from the superior olive. J Comp Neurol 2004;472:330–344. [PubMed: 15065128]

Long CJ, Eddington DK, Colburn HS, Rabinowitz WM. Binaural sensitivity as a function of interaural electrode position with a bilateral cochlear implant user. J Acoust Soc Am 2003;114:1565–1574. [PubMed: 14514210]

Macpherson EA, Middlebrooks JC. Listener weighting of cues for lateral angle: the duplex theory of sound localization revisited. J Acoust Soc Am 2002;111:2219–2236. [PubMed: 12051442]

Majdak P, Laback B, Baumgartner WD. Effects of interaural time differences in fine structure and envelope on lateral discrimination in electric hearing. J Acoust Soc Am 2006;120:2190–2201. [PubMed: 17069315]

Mardia, KV.; Jupp, PE. Directional Statistics. Chichester, UK: Wiley; 2000.

McAlpine D, Jiang D, Shackleton TM, Palmer AR. Convergent input from brainstem coincidence detectors onto delay-sensitive neurons in the inferior colliculus. J Neurosci 1998;18:6026–6039. [PubMed: 9671687]

Middlebrooks JC, Lee C. Cortical phase locking to sinusoidally modulated cochlear-implant pulse trains. Soc Neurosci Abstr 2004:529.4.

Moxon, EC. Electric stimulation of the cat's cochlea: a study of discharge rates in single auditory nerve fibers (S.M. thesis). Cambridge, MA: Massachusetts Institute of Technology; 1967.

Nelson PC, Carney LH. A phenomenological model of peripheral and central neural responses to amplitude-modulated tones. J Acoust Soc Am 2004;116:2173–2186. [PubMed: 15532650]

Oliver DL, Winer JA, Beckius GE, Saint Marie RL. Morphology of GABAergic neurons in the inferior colliculus of the cat. J Comp Neurol 1994;340:27–42. [PubMed: 7909821]

Pena JL, Konishi M. Auditory spatial receptive fields created by multiplication. Science 2001;292:249–252. [PubMed: 11303092]

Qin MK, Oxenham AJ. Effects of simulated cochlear-implant processing on speech reception in fluctuating maskers. J Acoust Soc Am 2003;114:446–454. [PubMed: 12880055]

Rubinstein JT, Wilson BS, Finley CC, Abbas PJ. Pseudospontaneous activity: stochastic independence of auditory nerve fibers with electrical stimulation. Hear Res 1999;127:108–118. [PubMed: 9925022]

Sakitt B. Indices of discriminability. Nature 1973;241:133–134. [PubMed: 4695543]

Schreiner CE, Langner G. Periodicity coding in the inferior colliculus of the cat. II. Topographical organization. J Neurophysiol 1988;60:1823–1840. [PubMed: 3236053]

Shackleton TM, Skottun BC, Arnott RH, Palmer AR. Interaural time difference discrimination thresholds for single neurons in the inferior colliculus of guinea pigs. J Neurosci 2003;23:716–724. [PubMed: 12533632]

Shannon RV. Multichannel electrical stimulation of the auditory nerve in man. II. Channel interaction. Hear Res 1983;12:1–16. [PubMed: 6689326]

Shannon RV, Zeng FG, Kamath V, Wygonski J, Ekelid M. Speech recognition with primarily temporal cues. Science 1995;270:303–304. [PubMed: 7569981]

Simpson AJ, Fitter MJ. What is the best index of detectability? Psychol Bull 1973;80:481–488.

Smith, ZM.; Delgutte, B. Binaural interactions with bilateral electric stimulation of the cochlea: evoked potential and single-unit measures; Association for Research in Otolaryngology Midwinter Meeting; Daytona Beach, FL. 2003a.

Smith, ZM.; Delgutte, B. Neural sensitivity to interaural timing differences with bilateral electric stimulation of the cochlea; Conference on Implantable Auditory Prosthesis; Pacific Grove, CA. 2003b.

Smith, ZM.; Delgutte, B. Binaural interactions in the auditory midbrain with bilateral cochlear implants; Association for Research in Otolaryngology Midwinter Meeting; New Orleans, LA. 2005a.

Smith, ZM.; Delgutte, B. What to do with the "where": a physiologically inspired strategy for delivering interaural timing cues with bilateral cochlear implants; Conference on Implantable Auditory Prosthesis; Pacific Grove, CA. 2005b.

Smith ZM, Delgutte B. Sensitivity to interaural time differences in the inferior colliculus with bilateral cochlear implants. J Neurosci 2007;27:6740–6750. [PubMed: 17581961]

Smith ZM, Delgutte B, Oxenham AJ. Chimaeric sounds reveal dichotomies in auditory perception. Nature 2002;416:87–90. [PubMed: 11882898]

Snyder R, Leake P, Rebscher S, Beitel R. Temporal resolution of neurons in cat inferior colliculus to intracochlear electrical stimulation: effects of neonatal deafening and chronic stimulation. J Neurophysiol 1995;73:449–467. [PubMed: 7760111]

Snyder RL, Vollmer M, Moore CM, Rebscher SJ, Leake PA, Beitel RE. Responses of inferior colliculus neurons to amplitude-modulated intracochlear electrical pulses in deaf cats. J Neurophysiol 2000;84:166–183. [PubMed: 10899194]

Tollin, DJ. Interaural level difference discrimination thresholds and virtual acoustic space minimum audible angles for single neurons in the lateral superior olive. In: Kollmeier, B.; Klump, G.; Hohmann, V.; Langemann, U.; Mauermann, M.; Uppenkamp, S.; Verhey, J., editors. Hearing—From Sensory Processing to Perception. Berlin: Springer; 2007. p. 425-434.

Tollin DJ, Yin TC. Interaural phase and level difference sensitivity in low-frequency neurons in the lateral superior olive. J Neurosci 2005;25:10648–10657. [PubMed: 16291937]

van de Par S, Kohlrausch A. A new approach to comparing binaural masking level differences at low and high frequencies. J Acoust Soc Am 1997;101:1671–1680. [PubMed: 9069634]

van den Honert C, Stypulkowski PH. Single fiber mapping of spatial excitation patterns in the electrically stimulated auditory nerve. Hear Res 1987;29:195–206. [PubMed: 3624083]

van Hoesel RJ. Sensitivity to binaural timing in bilateral cochlear implant users. J Acoust Soc Am 2007;121:2192–2206. [PubMed: 17471733]

van Hoesel RJ, Tyler RS. Speech perception, localization, and lateralization with bilateral cochlear implants. J Acoust Soc Am 2003;113:1617–1630. [PubMed: 12656396]

Wightman FL, Kistler DJ. The dominant role of low-frequency interaural time differences in sound localization. J Acoust Soc Am 1992;91:1648–1661. [PubMed: 1564201]

Wilson BS, Finley CC, Lawson DT, Wolford RD, Eddington DK, Rabinowitz WM. Better speech recognition with cochlear implants. Nature 1991;352:236–238. [PubMed: 1857418]

Xu SA, Shepherd RK, Chen Y, Clark GM. Profound hearing loss in the cat following the single co-administration of kanamycin and ethacrynic acid. Hear Res 1993;70:205–215. [PubMed: 8294265]

Yin TC, Chan JC. Interaural time sensitivity in medial superior olive of cat. J Neurophysiol 1990;64:465–488. [PubMed: 2213127]

Yin TC, Kuwada S. Binaural interaction in low-frequency neurons in inferior colliculus of the cat. III. Effects of changing frequency. J Neurophysiol 1983;50:1020–1042. [PubMed: 6631459]

Yin TC, Kuwada S, Sujaku Y. Interaural time sensitivity of high-frequency neurons in the inferior colliculus. J Acoust Soc Am 1984;76:1401–1410. [PubMed: 6512102]

Zurek, PM. Binaural advantages and directional effects in speech intelligibility. In: Studebaker, GA.; Hochberg, I., editors. Acoustical Factors Affecting Hearing Aid Performance. Boston, MA: Allyn and Bacon; 1993. p. 255-276.

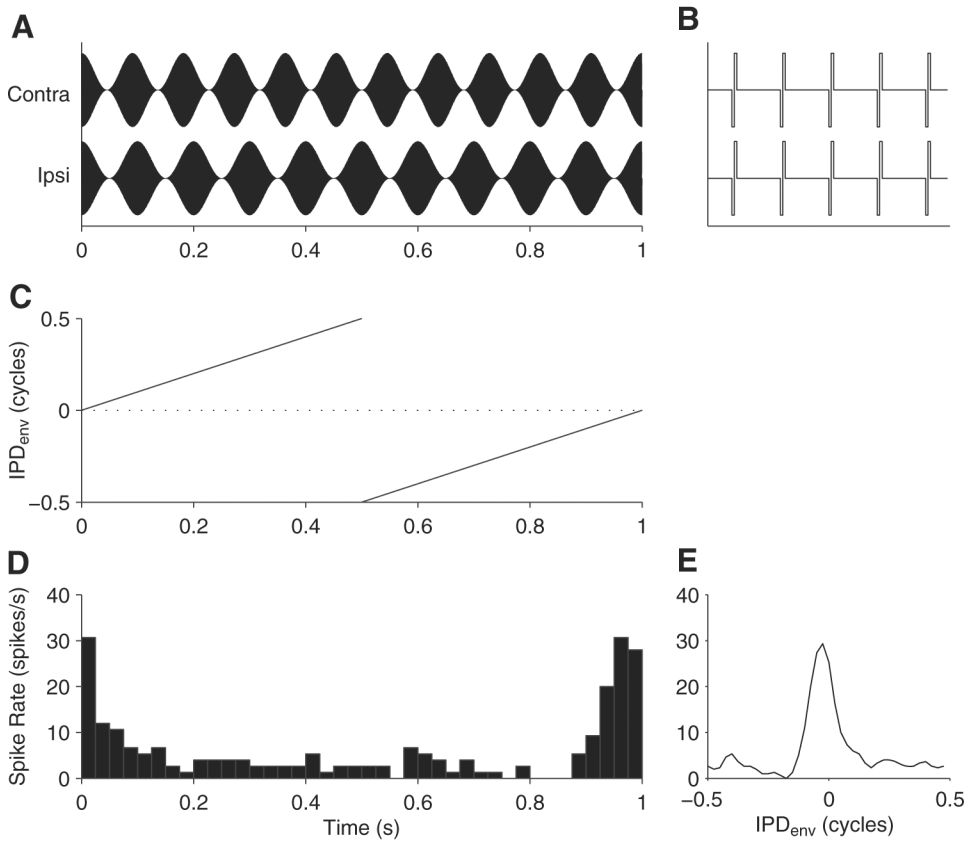

FIG. 1.

Binaural modulation beat (BMB) stimulus and example response from an inferior colliculus (IC) neuron. *A*: BMB stimulus. The modulation frequency in the contralateral ear is 1 Hz above that in the ipsilateral ear to create a dynamic interaural time difference in the envelope (ITD_{env}) that traverses the full range of interaural phase difference in the amplitude envelope (IPD_{env}; between −0.5 and 0.5 cycle) every second. For illustrative purposes, the modulation frequencies shown here are relatively low (11 Hz for the contralateral ear and 10 Hz for the ipsilateral ear). *B*: detailed (5-ms span) view of the stimulus waveforms shows that the carrier pulses are synchronized at the 2 ears (ITD_{fs} = 0 μs). *C*: IPD_{env} as a function of time for the BMB stimulus. *D*: period histogram of the response of a neuron to 30 s of stimulation by the BMB. Because the spike rate changes over time in synchrony with IPD_{env}, this neuron is sensitive to IPD_{env}. *E*: IPD_{env} tuning function obtained from response in *D*.

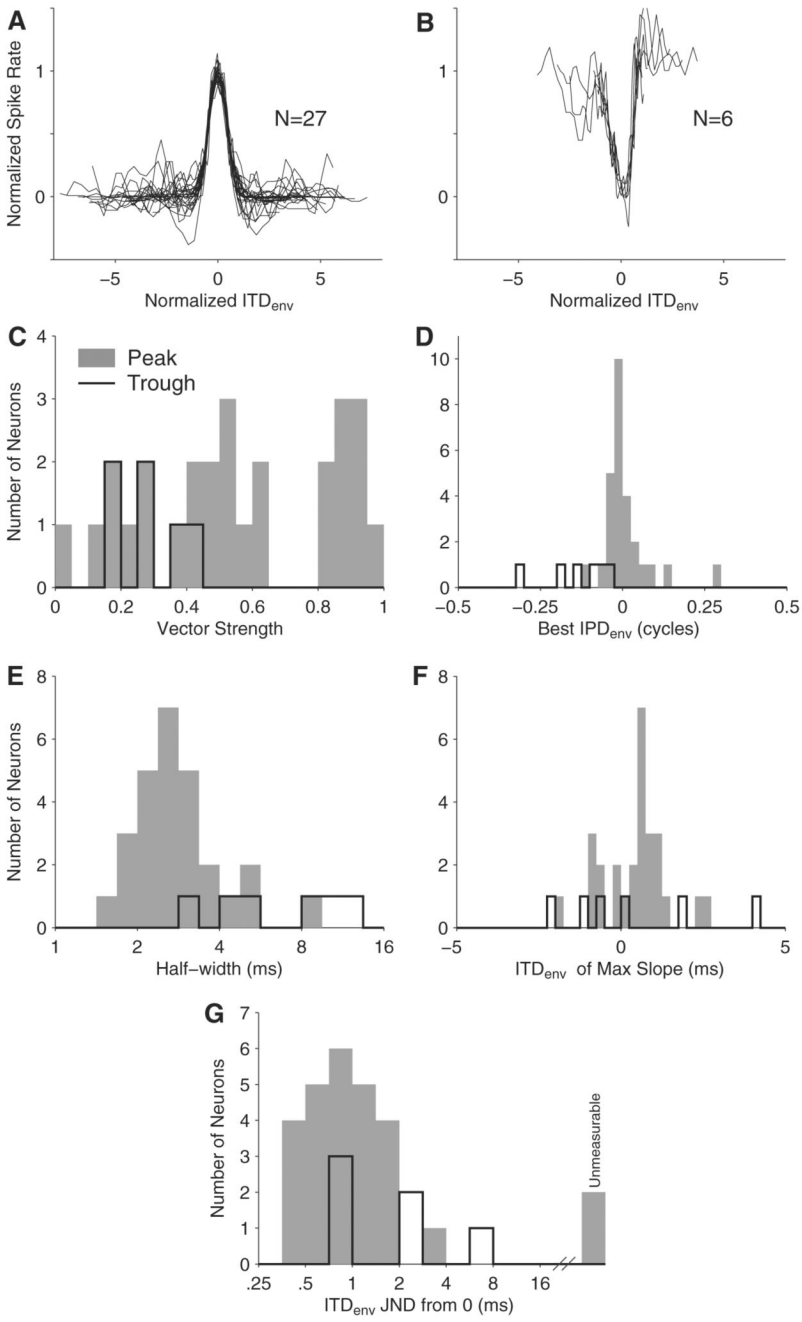

FIG. 2.

ITD$_{env}$ tuning for the standard BMB stimulus (pulse rate = 1,000 pps, f_{mod} = 40 Hz) across the population of ITD$_{env}$-sensitive IC neurons. *A* and *B*: normalized ITD$_{env}$ functions for all neurons tested (1 trace per neuron) with the standard BMB stimulus. Peak-shaped tuning is shown in *A* and trough-shaped tuning in *B*. Responses are scaled and shifted along both axes to show the goodness of fit of the positive and negative Gaussians to the data. *C*–*G*: distributions of vector strength, best IPD$_{env}$, ITD$_{env}$ half-width, maximum slope of ITD$_{env}$ tuning, and neural ITD$_{env}$ just noticeable differences (JNDs) for neurons with peak- and trough-shaped ITD$_{env}$ tuning. *G*: single-unit neural ITD$_{env}$ JNDs (from a reference of 0 ms) were measured in 31 of

33 neurons. The remaining 2 neurons with unmeasurable JNDs are shown to the right of the distributions.

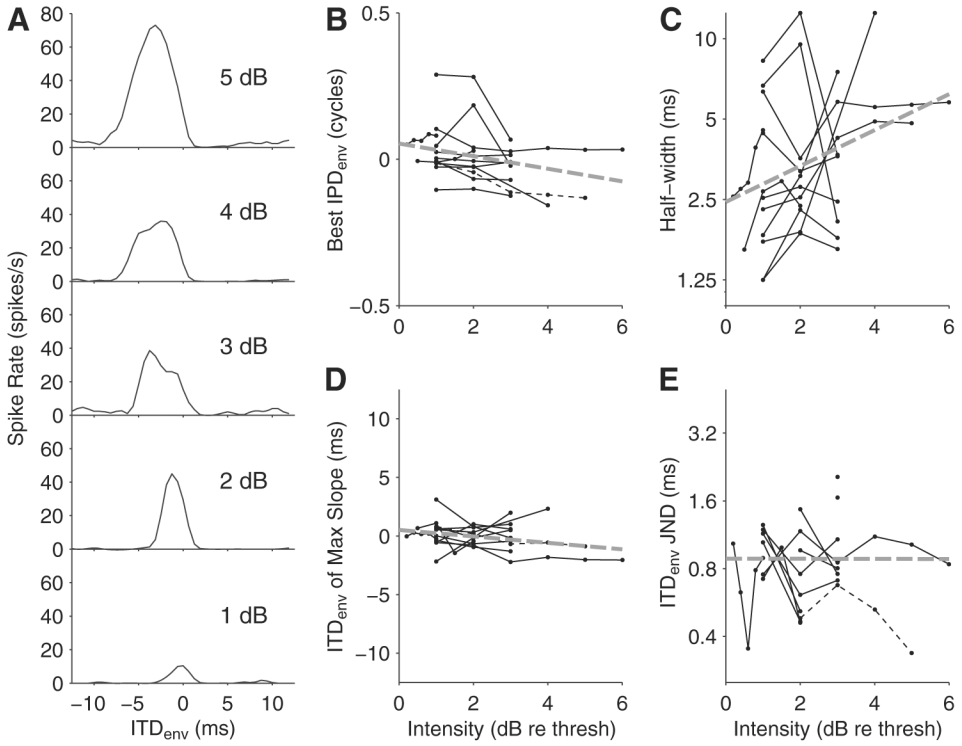

FIG. 3.

Effect of stimulus intensity on envelope ITD tuning. *A*: ITD_{env} functions for an IC neuron at 5 different stimulus intensities (units are dB re threshold; threshold is 0.71 mA peak amplitude). The stimulus is a binaural modulation beat with a 1,000 pps carrier and 40 Hz AM. *B–E*: best IPD_{env}, ITD_{env} half-width, ITD_{env} of maximum slope, and neural ITD_{env} JND as a function of intensity for 12 neurons. Thin lines show data from individual neurons and thick dashed lines are linear fits to the population data. The thin dashed lines are the data from the neuron in *A*.

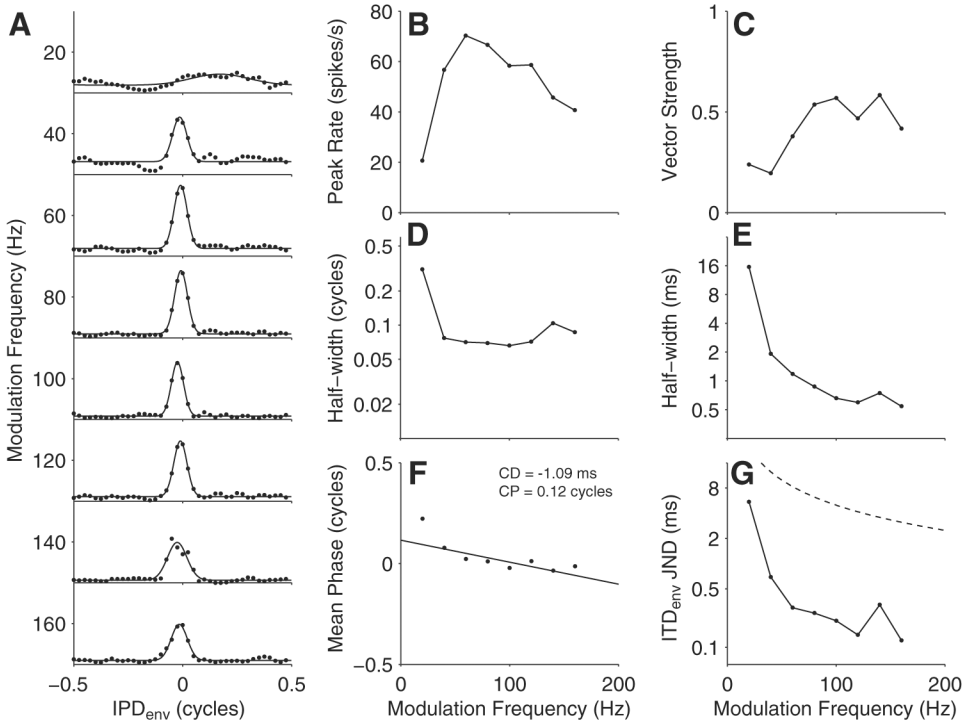

FIG. 4.

ITD$_{env}$ tuning at 8 different modulation frequencies for an example neuron. *A*: IPD$_{env}$ tuning curves for each f_{mod}.●, the measured data; —, Gaussian fits. The vertical axis is spike rate and the same scale is used for all 8 plots. *B*: peak spike rate as a function of f_{mod}. *C–G*: summary metrics from the data in *A* as a function of f_{mod}: vector strength (*C*), ITD$_{env}$ half-width in units of cycles of the modulation period (*D*), ITD$_{env}$ half-width in ms (*E*), mean interaural phase (*F*), and neural ITD$_{env}$ JNDs (*G*). Line in *F* is the weighted least-squares fit to the phase data used to estimate characteristic delay and phase (CD and CP). - - - in *G* indicates half of the modulation period, which is the upper limit of measurable ITD$_{env}$ JNDs.

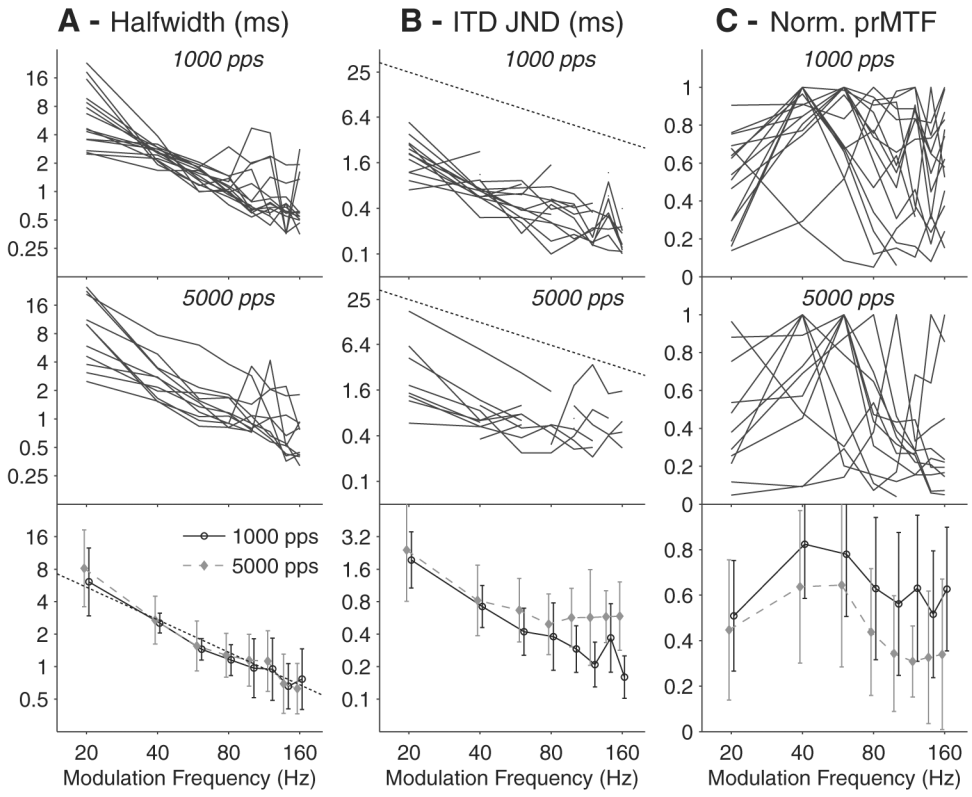

FIG. 5.

Effect of modulation frequency and carrier rate on envelope ITD tuning. *Top row*: single neuron data (n = 15) for carrier rate of 1,000 pps. *Middle row*: single neuron data (n = 11) for carrier rate of 5,000 pps. *Bottom row*: mean values across the neural population for the two carrier rates, error bars show ±1 SD. *A*: ITD_{env} half-width as a function of modulation frequency. The thin dotted line in the bottom panel is κ/f_{mod} (κ = 0.11). *B*: ITD_{env} JNDs as a function of modulation frequency. Thin dotted lines show upper limit of measurable values. Population mean JNDs only include measurable JNDs from single neurons. See Fig. 6*A* for the proportion of measurable JNDs at each f_{mod}. *C*: peak firing rate of IPD_{env} curve as a function of modulation frequency. Rates are normalized to their maximum.

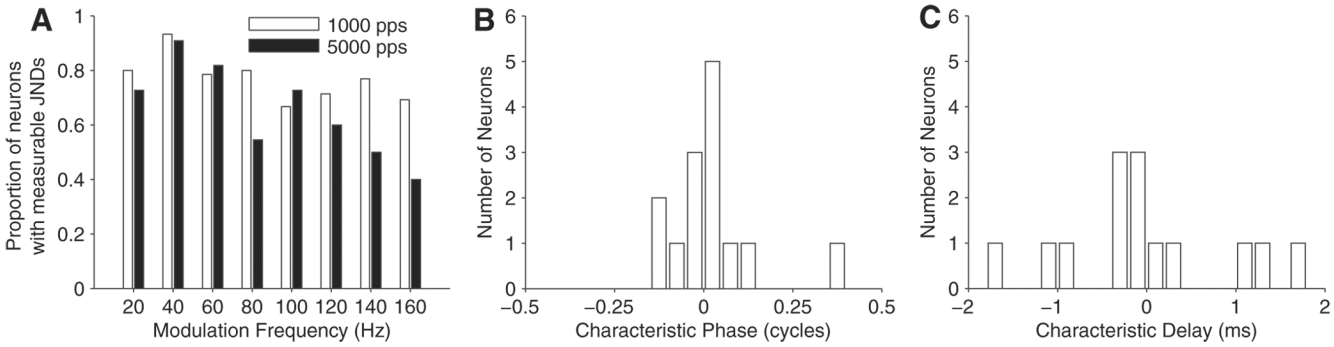

FIG. 6.

A: proportion of neurons with measurable ITD_{env} JNDs at different modulation frequencies. *B* and *C*: distributions of CP (*B*) and CD (*C*) calculated over f_{mod} from 20 to 160 Hz with a carrier rate of 1,000 pps (14/15 neurons had a linear phase-f_{mod} relationship and were included in this analysis).

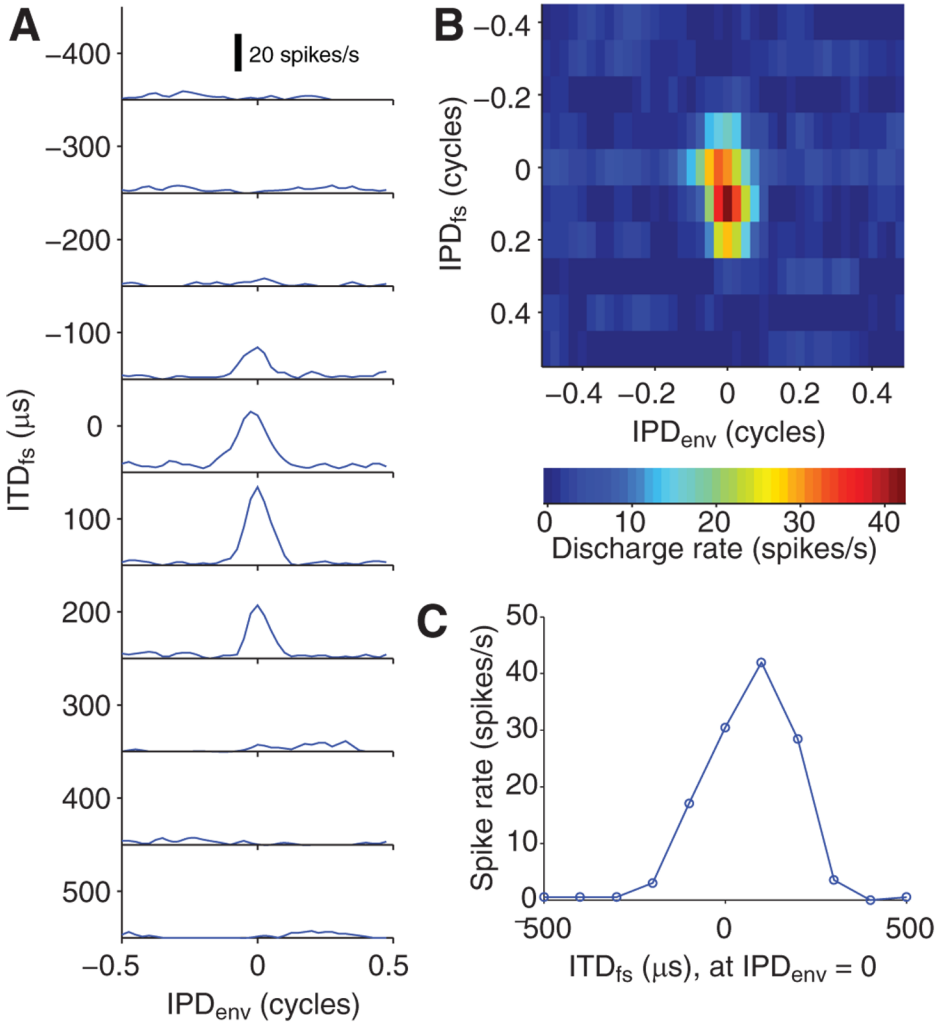

FIG. 7.

Sensitivity to fine structure ITD. *A*: IPD_{env} tuning curves at for 10 different fine structure ITD (ITD_{fs}). *B*: joint IPD_{env}-IPD_{fs} tuning function derived from data in *A*. *C*: ITD_{fs} tuning at $IPD_{env} = 0$.

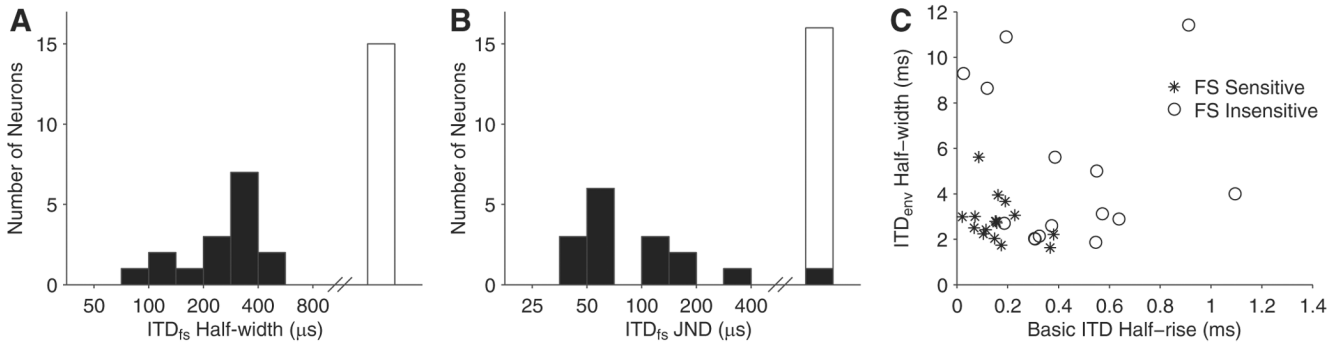

FIG. 8.

Characteristics of ITD_{fs} sensitivity across IC population for 1,000-pps carrier and 40-Hz modulation. *A*: distribution of ITD_{fs} half-widths. ■, ITD_{fs}-sensitive neurons; □, ITD_{fs}-insensitive neurons. *B*: distribution of neural ITD_{fs} JNDs. *C*: scatter plot of half-rise of ITD tuning for 40 pps constant-amplitude pulse trains (Smith and Delgutte 2007) against ITD_{env} half-width at 40 Hz. *, ITD_{fs}-sensitive neurons; ○, ITD_{fs}-insensitive neurons for the 1,000-pps carrier.

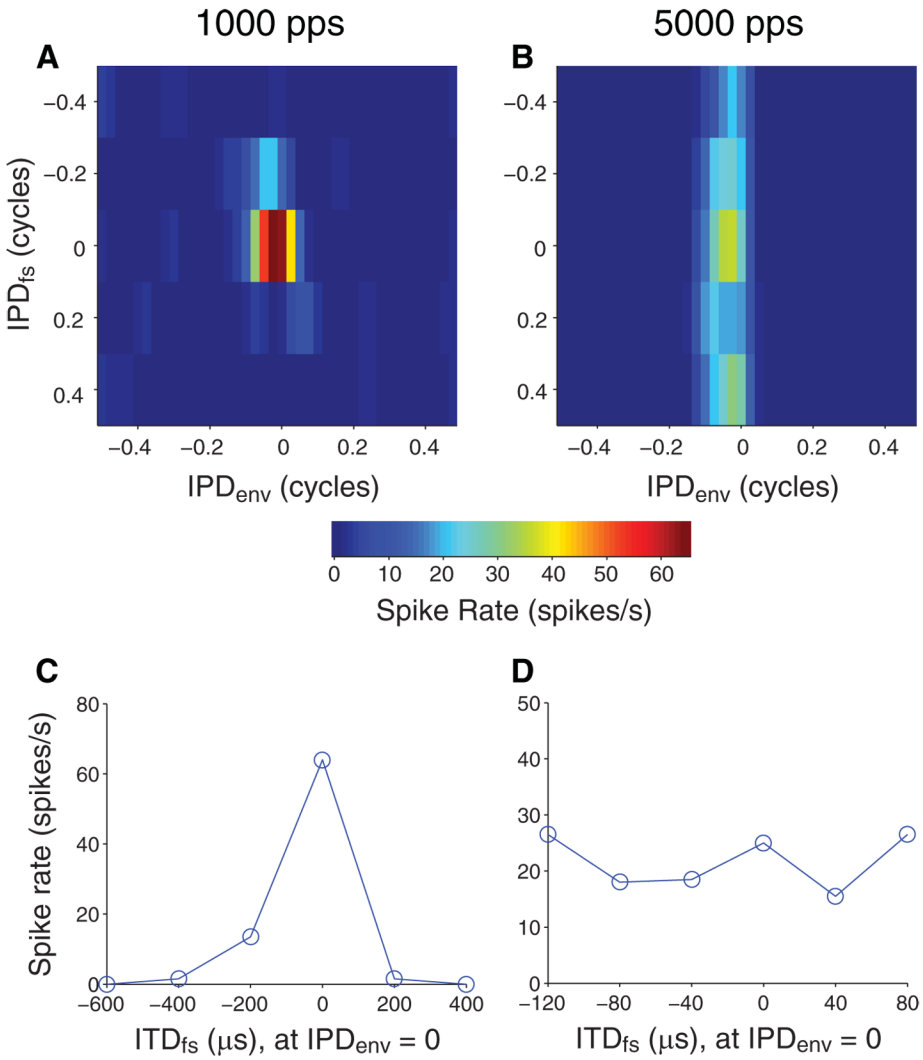

FIG. 9.

Effect of carrier rate on ITD_{fs} tuning. *A* and *B*: joint IPD_{env}-IPD_{fs} tuning function for a neuron at a pulse rate of 1,000 pps (*A*) and 5,000 pps (*B*). f_{mod} was 40 Hz in both cases. *C* and *D*: ITD_{fs} tuning at IPD_{env} = 0 for 1,000 pps (*C*) and 5,000 pps (*D*).

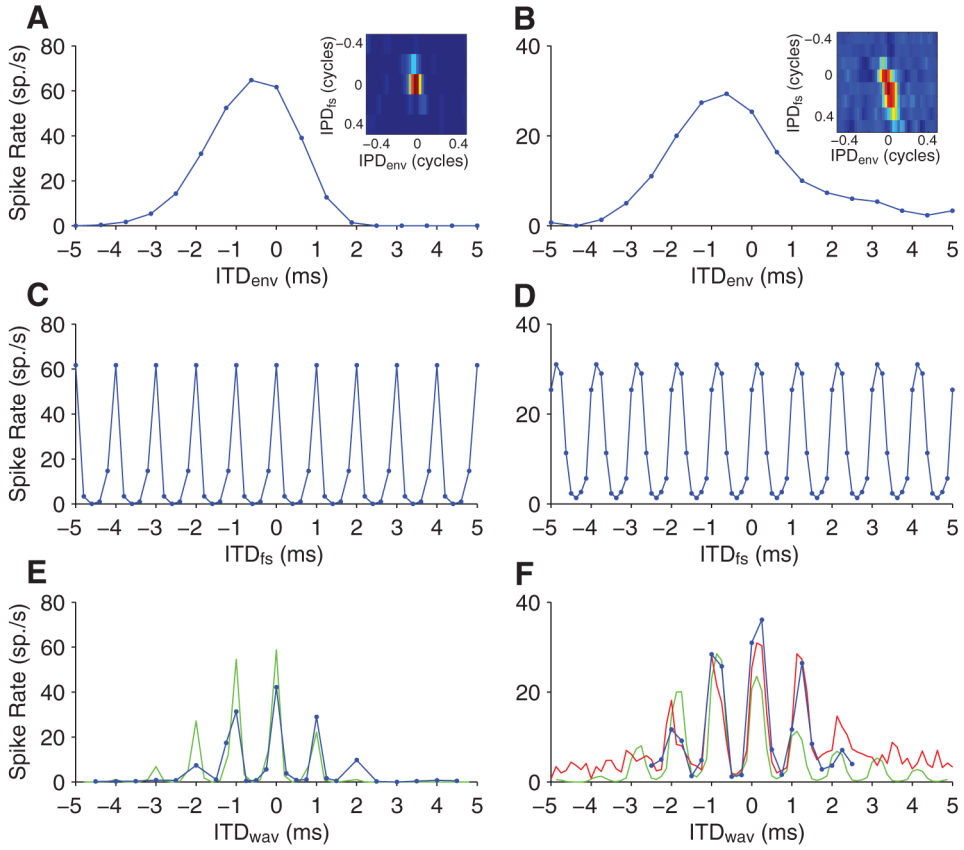

FIG. 10.

Sensitivity to ITD in the whole waveform for 2 neurons using a 1,000-pps, 40-Hz AM pulse train. *Left*: neuron is the same neuron as in Fig. 9. *A* and *B*: ITD_{env} tuning for ITD_{fs} fixed at 0. *Insets*: joint ITD_{env}-ITD_{fs} tuning functions. *C* and *D*: ITD_{fs} tuning for ITD_{env} fixed at 0. *E* and *F*: tuning to ITD in the whole waveform (ITD_{wav}). Blue points are direct measurements, green lines show predictions of ITD_{wav} tuning from multiplication of ITD_{env} and ITD_{fs} tuning curves, and the red line (*F* only) shows predictions of ITD_{wav} tuning from resampling the joint ITD_{env}-ITD_{fs} tuning function.

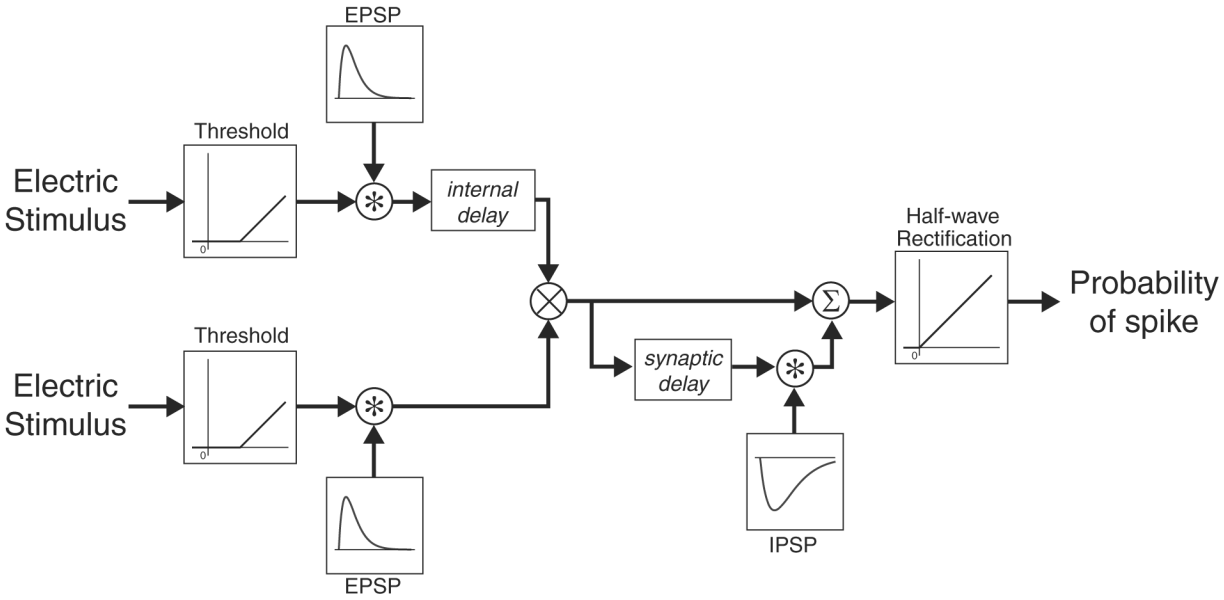

FIG. 11.

Phenomenological model of electric ITD tuning. Operations are shown in circles and include convolution (*), multiplication (×), and summation (∑).

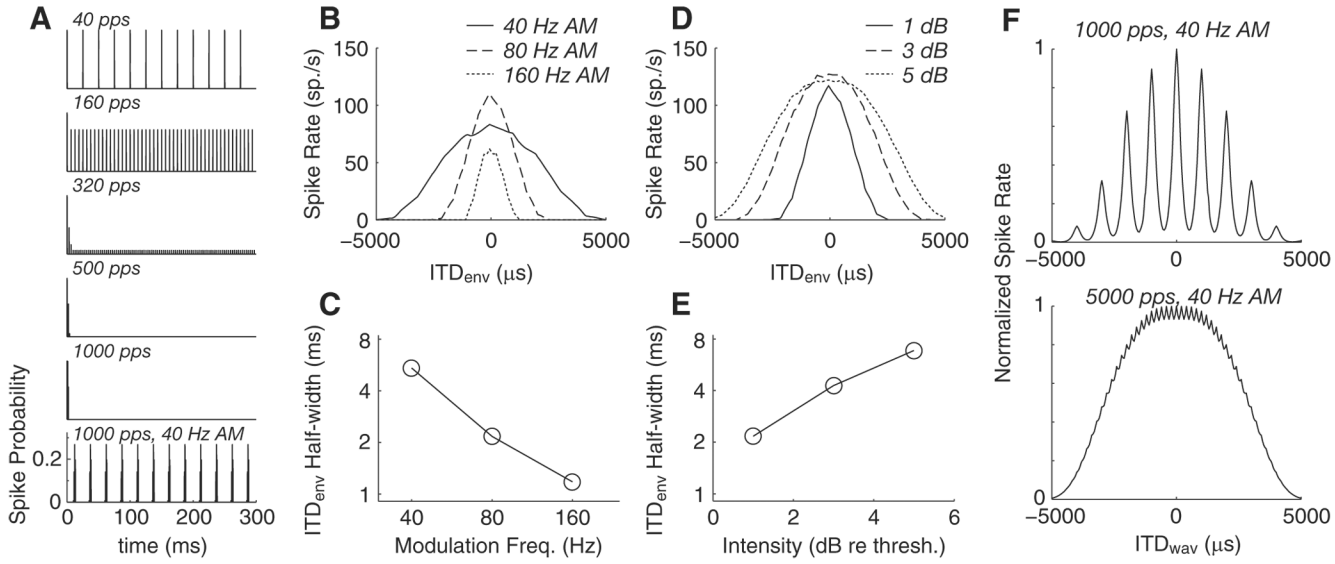

FIG. 12.

Responses of phenomenological model to various ITD stimuli. *A*: temporal response patterns for constant-amplitude pulse trains as a function of pulse rate. All stimuli are 300 ms in duration, the peak intensity is 1 dB re model threshold, and the ITD equals the model neuron's *internal delay* (ITD_{best}). The *bottom trace* shows the effect of 40-Hz AM on the response to a 1,000-pps pulse train. *B*: ITD_{env} tuning for a 1,000-pps AM stimulus at 3 modulation frequencies (1 dB re threshold). *C*: ITD_{env} half-width decreases with increasing modulation frequency. *D*: ITD_{env} tuning for a 1,000-pps, 80-Hz AM stimulus at 3 stimulus intensities (dB re threshold). *E*: ITD_{env} half-width increases with increasing intensity. *F*: model ITD_{wav} tuning for 1,000-pps, 40-Hz AM stimulus (*top*) and 5,000-pps, 40-Hz AM stimulus (*bottom*) at 1 dB re threshold.

TABLE 1

Number of neurons responsive to AM stimuli and sensitive to ITD

	Sustained Response to AM (any f_{mod})	Sensitive to Envelope ITD (any f_{mod})	Sensitive to Fine Structure ITD (1000 pps)	Sensitive to Fine Structure ITD (5000 pps)
Yes	46	35	17	1
Total Tested	47	46	31	7

Each successive column is a subset from the “yes” row of the previous column. AM, amplitude modulated; ITD, interaural time difference.

TABLE 2

Difference in basic ITD tuning between ITD_{fs}-sensitive and -insensitive neurons

	Basic Half-Rise, μs	Basic $\lvert ITD_{MS} \rvert$, μs	Physiological Modulation Depth, %	ITD_{env} Half-Width, ms	Electrode Depth, μm
ITD_{fs} sensitive (16)	161 ± 98	143 ± 173	84.8 ± 21.7	2.83 ± 0.97	2213 ± 740
ITD_{fs} insensitive (15)	436 ± 292	398 ± 372	51.3 ± 27.4	4.95 ± 3.42	2711 ± 563
Significance	$P = 0.0013$	$P = 0.019$	$P < 0.001$	$P = 0.024$	$P = 0.045$

Numbers are means ± SD. *P* values are from two-sample *t*-tests comparing properties of ITD_{fs}-sensitive and -insensitive units.

TABLE 3

Parameter values used in the phenomenological model of ITD tuning

Parameter	Value
τ_e, ms	0.1
τ_i, ms	2.0
α_e/α_i	1.25
Synaptic delay, ms	1.0